TECHNICAL REPORT STANDARD TITLE PAGE

1. Report No.	2. Government Accession No.	3. Recipient's Catalog No.
FHWA/TX-90+1190-2F		

4. Title and Subtitle	5. Report Date
TRUCK TIRE PAVEMENT CONTACT PRESSURE DISTRIBUTION CHARACTERISTICS FOR THE BIAS GOODYEAR 18-22.5, THE RADIAL MICHELIN 275/80R/24.5, THE RADIAL MICHELIN 255/70R/22.5, AND THE RADIAL GOODYEAR 11R24.5 TIRES	September 1989
	6. Performing Organization Code
7. Author(s)	8. Performing Organization Report No.
Rafael F. Pezo, Kurt M. Marshek, and W. R. Hudson	Research Report 1190-2F
9. Performing Organization Name and Address	10. Work Unit No.
Center for Transportation Research The University of Texas at Austin Austin, Texas 78712-1075	11. Contract or Grant No. Research Study 3-8-88/9-1190
	13. Type of Report and Period Covered
12. Sponsoring Agency Name and Address	Final
Texas State Department of Highways and Public Transportation Transportation Planning Division P. O. Box 5051 Austin, Texas 78763-5051	14. Sponsoring Agency Code

15. Supplementary Notes

Study conducted in cooperation with the U. S. Department of Transportation, Federal Highway Administration.

Research Study Title: "Tire Contact Pressure Distributions"

16. Abstract

This report presents the results of an experimental investigation into the contact areas and tire contact pressure distributions produced by statically loaded truck tires. For this report, the bias Goodyear 18-22.5 LR-H tire, the radial Michelin 275/80R/24.5 LR-G tire, the radial Michelin 255/70R/22.5 LR-G tire, and the radial Goodyear 11R24.5 LR-G tire were tested.

The testing consisted of making contact pressure and contact area prints at the interface between the tire and a steel plate at different wheel loads and tire inflation pressures. The pressure prints were produced using Fuji prescale film. The Fuji prescale film produces color variations, when pressure is applied to it, in such a way that darker pigmentation is produced in zones of higher pressure. The variations in color intensities of the Fuji film prints are related to contact pressure values produced for the film color calibration curve. Then, by digitizing the images and using computer software developed exclusively for this project, the tire contact pressure distributions were determined. The proportions of contact area covered by the various pressure ranges were computed and compared in order to observe the patterns and to estimate the significance of high contact pressures.

The contact area prints were made by applying ink to the tire and pressing the tire over a white paper that covered the steel plate. The ink prints have only one color and were used for calculating the tire-plate contact areas. Also, the side tire movements were measured for the tires during testing to allow other researchers to relate subsequent theoretical studies to our experimental results.

This report also proposes mathematical models for (1) estimating the tire contact area based on the relative area value (ratio of wheel load over inflation pressure) and (2) estimating the tire vertical stiffness based on the tire contact area.

17. Key Words	18. Distribution Statement
tire pressures, truck tires, contact area, contact pressure distributions, axle loads, pavements, side tire movements, tire deflections, tire vertical stiffness	No restrictions. This document is available to the public through the National Technical Information Service, Springfield, Virginia 22161.

19. Security Classif. (of this report)	20. Security Classif. (of this page)	21. No. of Pages	22. Price
Unclassified	Unclassified	56	

Form DOT F 1700.7 (8-69)

TRUCK TIRE PAVEMENT CONTACT PRESSURE DISTRIBUTION CHARACTERISTICS FOR THE BIAS GOODYEAR 18-22.5, THE RADIAL MICHELIN 275/80R/24.5, THE RADIAL MICHELIN 255/70R/22.5, AND THE RADIAL GOODYEAR 11R24.5 TIRES

by

Rafael F. Pezo
Kurt M. Marshek
W. R. Hudson

Research Report Number 1190-2F

Research Project 3-8-88/9-1190

Tire Contact Pressure Distributions

conducted for

Texas State Department of Highways and Public Transportation

in cooperation with the

U.S. Department of Transportation Federal Highway Administration

by the

CENTER FOR TRANSPORTATION RESEARCH

Bureau of Engineering Research
THE UNIVERSITY OF TEXAS AT AUSTIN

September 1989

The contents of this report reflect the views of the authors, who are responsible for the facts and the accuracy of the data presented herein. The contents do not necessarily reflect the official views or policies of the Federal Highway Administration. This report does not constitute a standard, specification, or regulation.

There was no invention or discovery conceived or first actually reduced to practice in the course of or under this contract, including any art, method, process, machine, manufacture, design or composition of matter, or any new and useful improvement thereof, or any variety of plant which is or may be patentable under the patent laws of the United States of America or any foreign country.

PREFACE

This is the second of two reports which describe work done on Project 1190, "Tire Contact Pressure Distributions." This study was conducted at the Center for Transportation Research (CTR), The University of Texas at Austin, as part of a cooperative research program sponsored by the Texas State Department of Highways and Public Transportation.

Many people contributed toward the completion of this report. Thanks are expressed to Dr. Tom Tielking for his input, to Mr. Larry Walker of Walker Tire Company for providing the tires, to Ms. Peggy Johnson, and to CTR personnel, especially Lyn Antoniotti and Carl Bertrand.

We acknowledge their contributions and greatly appreciate their efforts in making this a successful project.

Rafael F. Pezo
Kurt M. Marshek
W. R. Hudson

September 1989

LIST OF REPORTS

Report No. 1190-1, "Truck Tire-Pavement Contact Pressure Distributions for Super Single 18-22.5 and Smooth 11R24.5 Tires," by Rex William Hansen, Carl Bertrand, Kurt M. Marshek, and W. R. Hudson, presents experimental data on the effect of tire inflation pressure and static wheel load on contact pressure distributions for the bias Goodyear 18-22.5 and the smooth radial Armstrong 11R24.5 tires. July 1989

Report No. 1190-2F, "Truck Tire Pavement Contact Pressure Distribution Characteristics for the Bias Goodyear 18-22.5, the Radial Michelin 275/80R/24.5, the Radial Michelin 255/70R/24.5, and the Radial Goodyear 11R24.5 Tires," by Rafael F. Pezo, Kurt M. Marshek, and W. R. Hudson, presents experimental data on the effect of tire inflation pressure and static wheel load on contact pressure distribution, contact area, tire deflections, and tire vertical stiffness. September 1989.

ABSTRACT

This report presents the results of an experimental investigation into the contact areas and tire contact pressure distributions produced by statically loaded truck tires. For this report, the bias Goodyear 18-22.5 LR-H tire, the radial Michelin 275/80R/24.5 LR-G tire, the radial Michelin 255/70R/22.5 LR-G tire, and the radial Goodyear 11R24.5 LR-G tire were tested.

The testing consisted of making contact pressure and contact area prints at the interface between the tire and a steel plate at different wheel loads and tire inflation pressures. The pressure prints were produced using Fuji prescale film. The Fuji prescale film produces color variations, when pressure is applied to it, in such a way that darker pigmentation is produced in zones of higher pressure. The variations in color intensities of the Fuji film prints are related to contact pressure values produced for the film color calibration curve. Then, by digitizing the images and using computer software developed exclusively for this project, the tire contact pressure distributions were determined. The proportions of contact area covered by the various pressure ranges were computed and compared in order to observe the patterns and to estimate the significance of high contact pressures.

The contact area prints were made by applying ink to the tire and pressing the tire over a white paper that covered the steel plate. The ink prints have only one color and were used for calculating the tire-plate contact areas. Also, the side tire movements were measured for the tires during testing to allow other researchers to relate subsequent theoretical studies to our experimental results.

This report also proposes mathematical models for (1) estimating the tire contact area based on the relative area value (ratio of wheel load over inflation pressure) and (2) estimating the vertical stiffness based on the tire contact area.

SUMMARY

The rate of deterioration of highway pavements over the last 50 years has been accelerating. During this time, legal truck sizes, weights, wheel loads and tire inflation pressures have increased. This report describes a study which seeks to measure actual tire-pavement contact pressure distributions, in order to provide pavement designers with estimates of tire pressure for use in studies of pavement deterioration and to assist legislators in developing legislation regarding tire usage.

This report presents the results of an experimental study involving several truck tires statically loaded against a steel plate. The bias Goodyear 18-22.5 LR-H "super single" tire, the radial Michelin 275/80R/24.5 LR-G tire, the radial Michelin 255/70R/22.5 LR-G tire, and the radial Goodyear 11R24.5 LR-G were tested and studied for this report. These tires were chosen because they are popular for use on Texas highways.

The testing consisted of making contact pressure measurements and contact area prints at the interface between the tire and the support plate at different wheel loads and tire inflation pressures. The pressure prints were produced using Fuji prescale film. The Fuji prescale film produces a color variation when pressure is applied to it, in such a way that darker pigmentation is produced in zones of higher pressure. The variations in color intensities of the Fuji film prints are related to actual contact pressure values produced for the film color calibration curve. Then, by digitizing the images and using computer software developed exclusively for this project, the tire contact pressure distributions were determined. The proportions of contact area covered by the various pressure ranges were computed and compared in order to observe the patterns and to estimate the significance of high contact pressures.

The contact area prints were made by applying ink to the tire and pressing the tire over a white paper that covered the steel plate. The ink prints have only one color and were used for calculating the tire-plate contact areas. Also, the side tire movements were measured during testing to allow other researchers to relate subsequent theoretical studies to our experimental results.

This report also proposes mathematical models for (1) estimating the tire contact area based on the relative area value (ratio of wheel load over inflation pressure) and (2) estimating the tire vertical stiffness based on the tire contact area.

The conclusions from this project can be summarized as follows: (1) for bias truck tires the shape of the contact area is generally circular with an oval tendency, while for radial truck tires the shape is consistently rectangular; (2) in general, for a constant tire inflation pressure, as the wheel load increases, the proportion of contact area increases for higher contact pressure ranges and decreases for lower contact pressure ranges; (3) similarly, for a constant wheel load, as the tire inflation pressure increases, the proportion of contact area increases for higher contact pressure ranges and decreases for lower contact pressure ranges.

IMPLEMENTATION STATEMENT

The results of this project provide tire contact areas, tire contact pressure distributions, and proportions of contact area covered by different pressure ranges for truck tires at several inflation pressures and wheel loads. These relationships can be used to evaluate the effects of truck tire inflation pressure and axle load on the structural capacity of pavements. The results can help to clarify many pressing problems, such as rutting, shoving, etc. Such information and evaluation leads to changes in methods employed in current pavement design to improve the performance of pavements and can also assist legislators in developing legislation regarding allowable tire pressures and related issues.

TABLE OF CONTENTS

PREFACE iii

LIST OF REPORTS iii

ABSTRACT iii

SUMMARY iv

IMPLEMENTATION STATEMENT iv

CHAPTER 1. INTRODUCTION

Background 1
Objectives 1
Scope and Organization of the Study 1
Research Approach 1

CHAPTER 2. REVIEW OF TIRE CONTACT PRESSURE STUDIES

Literature Survey 3
Tire-Pavement Interface Pressure Characteristics 3
Tire Contact Pressure and Its Effect on Pavement Performance 3
Future Trends in Tire Types 4
Conclusions 4

CHAPTER 3. EXPERIMENTAL PROCEDURES

Experimental Parameters 6
Tires 6
Loads and Inflation Pressures 6
Experimental Procedure 6
Mounting the Tire 6
Testing the Tire and Producing Calibration Squares 6
Analysis of the Fuji and Ink Prints 9
Presentations of Results 9

CHAPTER 4. EXPERIMENTAL RESULTS

Bias Goodyear 18-22.5 LR-H "Super Single" Tire 10
Radial Michelin 275/80R/24.5 LR-G Tire 10
Radial Michelin 255/70R/22.5 LR-G Tire 11
Radial Goodyear 11R24.5 LR-G Tire 16

CHAPTER 5. DISCUSSION AND ANALYSIS OF RESULTS

Tire Contact Area 39
Discussion of Results 39
Analysis of Results 39
Tire Contact Pressure Distributions 40
Proportions of Contact Area 40
Discussion 40
Analysis 40

Comparison Between the Tires 41
Load Distribution Along the Tread Width 42
Tire Vertical Stiffness 42
Discussion 42
Analysis of Results 42

CAHPTER 6. CONCLUSIONS AND RECOMMENDATIONS
Conclusions 44
Recommendations 44

REFERENCES 45

APPENDIX A. EXPERIMENTAL AND ANALYTICAL PROCEDURES FOR DETERMINING TIRE CONTACT PRESSURE DISTRIBUTIONS 47

APPENDIX B. SIDE TIRE MOVEMENT DATA 48

CHAPTER 1. INTRODUCTION

BACKGROUND

The rate of highway pavement deterioration has been observed to be accelerating over the last 50 years (Refs 26 and 27). A variety of factors have been identified as contributing to the accelerated rate of pavement damage, including increased truck weights, sizes, wheel loads, and tire inflation pressures. Tire contact pressure distribution and its eroding effect on the pavement has, until recently, received very little attention. It is now increasingly recognized that the tire-pavement contact pressure distribution is an important factor in pavement deterioration and, consequently, a major consideration in new pavement and rehabilitation design.

As the cost of fuel has increased, the trucking industry has sought ways to economize its operations. One approach was an attempt to improve truck gas mileage by reducing rolling resistance through the use of higher tire inflation pressures. This increased tire pressure has presumably caused an increase in the rutting and fatigue failures of asphaltic concrete pavements.

The AASHO Road Test was conducted and analyzed using 1958-1960 truck characteristics. Since then tire pressures have increased, and their effects on fatigue damage to pavements are not documented. Although pavement designers have in the past attempted to counteract the effects of increased loading through improved pavement and geometric designs, the rate of pavement deterioration continues to increase (Refs 6, 11, 15, and 23). The actual pavement loading mechanisms and their magnitudes must be identified in order to estimate real pavement performance.

Current pavement design assumes a uniform pressure distribution equal to the tire inflation pressure loaded over a circular tire contact area. Research has clearly demonstrated that the actual pressures are dependent on the user vehicle operating characteristics, tire type, wheel load, and tire inflation pressures.

Several attempts have been made to determine tire contact pressure distributions. Tielking (Ref 15), for example, developed a finite element model of tires to estimate stresses and strains in pavements when the tire is loaded and inflated to different air pressures. However, none of these studies has been related to and calibrated with experimental measurements.

At The University of Texas at Austin, contact pressure distributions of a statically loaded tire have been experimentally determined (Refs 1, 2, and 25). This has been possible through a system which provides numerical pressure values for the contact area and two-dimensional color spectrum graphics that clearly focus on the variations in contact pressures and show the locations of the peak pressure values.

OBJECTIVES

The objectives of the study described in this report are (1) to establish pressure distributions for four different types and sizes of tires in contact with a steel plate, (2) to provide data to assist pavement designers in estimating the increasing rate of highway deterioration, and (3) to provide legislators with information for use in developing legislation regarding tire pressure limits and usage.

SCOPE AND ORGANIZATION OF THE STUDY

Chapter 2 contains a brief summary of related studies dealing with this subject. A description of the experimental procedure used in this project is presented in Chapter 3. Chapter 4 contains the experimental results, including tire contact pressure distributions, contact areas, load distributions across the tread width, and proportions of contact area covered by different pressure ranges for the tires tested. A discussion and an analysis of the results are presented in Chapter 5, along with appropriate statistical analyses. In Chapter 6, conclusions and recommendations for future research are presented.

RESEARCH APPROACH

To identify the contact area and pressure magnitudes, static testing was performed at The University of Texas at Austin on several tires at various inflation pressures and wheel loads. These tires were a bias Goodyear 18-22.5 LR-H super single, a radial Michelin 275/80R/24.5 LR-G, a radial Michelin 255/70R/22.5 LR-G, and a radial Goodyear 11R24.5 LR-G.

The experimental procedure consisted of four stages: (1) mounting the tire, (2) testing the tire and producing calibration squares, (3) analyzing the Fuji and ink prints, and (4) presenting the results. Details of the experimental procedure can be found in Chapter 3 of this report.

In general, Fuji prescale film was the medium used to capture the tire contact pressure distributions. This is the film used by Hansen, Chan, and Marshek in References 1, 2, and 25. The Fuji prescale film was located between the tire and the steel plate. By applying different loads to the tire, the Fuji prints were produced. The Fuji prints were then scanned and digitized using an Adage 3006 Graphics system. Several computer programs written exclusively for this project were run in order to measure, analyze, and display the truck tire contact pressure distributions.

The tire contact area and the applied wheel load values obtained from the analysis of the Fuji prints were checked

for consistency. Tire contact areas were estimated by producing ink prints and analyzing them. The applied wheel loads were determined using the computer programs and compared with the actual applied loads used in testing. This checking process enhanced the validity of the results.

The truck tire pavement contact pressure distributions of the four tested tires are presented in two ways, in Chapter 4: (1) numerical pressure maps and (2) two-dimensional color pressure plots.

CHAPTER 2. REVIEW OF TIRE CONTACT PRESSURE STUDIES

This chapter discusses the literature associated with tire contact pressure distributions. Several technical publications related to tire contact pressures, wheel loads, tire types, and tire inflation pressures were reviewed. Descriptions of the tire-pavement interface pressure characteristics, their effect on pavement life, and future trends in tire types are presented below.

LITERATURE SURVEY

A literature search was conducted to determine the existing state of knowledge relating to the project. The reference collection of the Center for Transportation Research at The University of Texas at Austin, the Highway Department libraries in various states, and other academic libraries were among the sources of information for this project. This section presents a review of several papers addressing the problems of tire-pavement interface pressure characteristics and tire contact effects on pavement life.

Tire-Pavement Interface Pressure Characteristics

In pavement design, it is frequently assumed that (1) the tire contact pressure is equal to the tire inflation pressure, and (2) the tire contact pressure is uniformly distributed over a circular area. These assumptions are based on the idea that, if an inflated membrane is in contact with a flat surface, the contact pressure at each point is equal to the membrane's inflation pressure and the contact area is circular. Theoretically, as well as experimentally, it has been demonstrated that contact pressures are not uniform and contact areas are not circular. Models constructed with these assumptions are hardly accurate because carcass stiffness as well as stiffness in the sidewalls prohibits equal pressure distribution in the contact area (Ref 20).

Lippmann and Oblizajek (Ref 17) stated that tire pavement contact area is influenced by factors such as vehicle speed, wheel load, tire inflation pressures, wheel camber, steering, braking, vehicle suspension, and tire configuration. Tielking and Roberts (Ref 15) described the mechanism whereby a tire transfers a wheel load to the pavement. Tielking and Roberts stated that changes in either the wheel load or the tire inflation pressure result in variations in actual contact area.

Ginn and Marlowe (Ref 22) explained the characteristics of tire-pavement contact stresses, describing their components and orientations. The stresses can be represented by two components, one perpendicular and the other tangent to the contact surface. This latter component may also be subdivided into two sub-components, each lying in the contact plane. One of the two sub-components is parallel to the central plane of the tire and is called the longitudinal stress component; the other, called the lateral stress component, is perpendicular to the central plane of the tire. In general, these sub-components are called shear components.

The shear components are created when an inflated tire is deflected against the pavement, causing the doubly-curved surface of the tread to become a flat surface. When the tire is vertically deflected against a flat surface, the motion is restrained by friction between the tire and the pavement, creating perpendicular horizontal shear components of contact pressure. However, when the tire rolls freely without camber, the shear pressure is re-directed, due to the superposition of an angular velocity on the tread surface. Bonse and Kuhn (Ref 21) experimentally confirmed this as early as 1959 by rolling a tire over a circular force-measuring stud placed in a manhole cover.

Tielking and Roberts (Ref 15) believed that the magnitude of the lateral shear is dependent on tire construction, with the radial tires producing about one-half lower peak pressure values than bias tires. They also believed that the lateral shear pressure applies a much higher stress to the pavement than does longitudinal shear pressure.

Tire Contact Pressure and Its Effect on Pavement Performance

A pavement must provide the load-bearing surface for which it is designed. This depends on the expected traffic loads, density of traffic, and desired service life. The pavement must maintain an adequate surface condition such that it is able to permit comfortable and safe driving within the designated speed limits. The service life is dependant on the loading the pavement receives. Traditionally, pavement design engineers have been primarily concerned with only the wheel loading effects, but, recently, research efforts have also investigated environmental and traffic effects caused by wheel loads and tire inflation pressures. References 4, 15, 18, 27, 28, and 29 discuss the stress and strain relationship in an asphalt pavement system caused by wheel load and inflation pressure.

In general, the literature shows that the major causes for increases in pavement fatigue and rutting rates are increases in wheel loads and tire inflation pressures. For example, van Vuuren (Ref 4) analyzed various linear elastic pavement structures under many combinations of wheel loads and inflation pressures, using the Chevron computer program. He attributed four types of pavement failure to high contact pressure: (1) fatigue of the surface layer, (2) fatigue of cement stabilized bases, (3) surface densification, and (4) consolidation of the subgrade. Another researcher, Eisenmann (Ref 27), states that pavement rutting is caused by mechanical abrasion and is due to irreversible material

deformations. These deformations are mainly caused by high tire contact pressure concentrations, which are in turn caused by a change in wheel load and/or a change in tire inflation pressure. Papagianakis (Ref 18) likewise believes that the compressive strains at the top of the asphalt surface are dramatically affected by high tire inflation and contact pressures.

Many researchers have addressed this growing problem, the effects of tire contact pressures on pavement life. References 5, 18, and 26 describe possible pavement-life-saving solutions. For example, Brown (Ref 5), at a symposium for high pressure truck tires, stated that, through legislation and improved engineering, pavement life could possibly be maintained and extended. The possible legal measures he mentioned were (1) placing legal limits on tire pressures, (2) placing controls on the manufacture of high pressure tires, (3) requiring approval by FHWA of any new tire carcass design, (4) requiring approval for any new suspension system (considering tires as a component of the suspension system), and (5) using tire inflation pressure as a factor in setting truck user taxes.

Nine states have already implemented conditional provisions for the maximum wheel load as a function of the tire inflation pressure (Refs 6 and 16). These regulations are generally expressed as two allowable loads per tire, one for inflation pressures below 100 psi and another for inflation pressures above 100 psi.

The possible engineering improvements suggested by Brown include (1) the use of more accurate pavement structural design models, (2) possible development of better binders and cements, and (3) emphasis on better quality control and mix design criteria. These improvements, if implemented, will help in estimating the pavement performance and service life in a more reliable manner.

Future Trends in Tire Types

Pavement designers are concerned with future trends in tire types. For example, Papagianakis and Haas (Ref 18) mentioned that inflation pressures, regardless of tire types, are much higher than they were two decades ago. Yeager (Ref 19), based on the fact that radial tires have a demonstrated higher wear life, predicted that the amount of radial replacement tires would increase from 65 to 88 percent within the next 10 years. Yeager also stated that the average set of radial automotive tires currently serves for approximately 39,000 miles before replacement (some of the new designs are capable of 65,000 miles). Recently, with the introduction to the market of the all-season radial tire, traditional bias tires are being rapidly replaced.

Most experts agree that the popularity of radial tires will continue to grow, particularly the all-season radials. The all-season tire has proven to be fuel efficient and provides good traction on wet and snowy roads. The all-season tire, with its improved performance capability and lower profile, has become even more attractive.

Papagianakis (Ref 18) stated that tire manufacturers are attempting to improve tire uniformity and further reduce rolling resistance by modifying design and production procedures. Rolling resistance has also been reduced by increasing inflation pressures. This trend will continue with the widespread use of low-profile tires and variable comfort suspension systems.

Roberts (Ref 3), for example, used a tire inflation pressure of 125 psi in his model to estimate the behavior of thin asphalt concrete surfaces on granular bases. He said that, although 125 psi may appear high, representatives from various tire manufacturers indicate that within the next 5 years (1986-91) tire inflation pressures would continue to rise, to nearly 150 psi. He believed that higher tire inflation pressures resulted because increased fuel costs prompted the trucking industry to attempt to reduce rolling resistance and thereby increase fuel economy. Therefore, the tire manufacturers have responded by marketing both bias and radial tires that operate at higher tire inflation pressures.

Zekoski (Ref 23) believes radialization will continue into applications that traditionally have been bias dominated, to increase fuel economy (e.g., on school buses, pick-up trucks, and delivery trucks).

Zekoski also addressed the possible impact of European tires. There is a trend in Europe to manufacture tires having higher load capabilities and inflation pressures to meet the increasing regional legal load limits, which are higher than those in the U.S. He believed that, as the global marketplace continues to mature, an increasing number of these tires will enter the United States, and the effect of these tires on pavement life must be addressed.

CONCLUSIONS

From the literature review the following conclusions may be made:

(1) Wheel load and tire inflation pressure have a significant effect on pavement service life.

(2) The major causes for the increase in pavement fatigue and rutting rates are increases in the wheel loads and tire inflation pressures.

(3) Theoretically and experimentally it has been demonstrated that contact pressures are not uniform and that the contact area is not circular.

(4) Tire contact forces are normal stresses, and are longitudinal and lateral shear stresses.

(5) Factors affecting contact pressure distributions include speed, steering, tire camber, tire construction, braking, inflation pressure, and wheel load .

(6) The use of radial tires will increase significantly, replacing the bias tire market at a faster rate.

(7) Improved engineering and increased legislation may reduce pavement rutting and fatigue caused by high wheel loads and high inflation pressures.

These conclusions reinforce the need for the experimental determination of the tire contact pressure distributions, since these pressure distributions have a major influence on pavement performance and service life. As stated in Chapter 1, this report addresses this need by testing several popular tires and presenting the variations of tire contact pressures when a wheel load and/or a tire inflation pressure changes.

CHAPTER 3. EXPERIMENTAL PROCEDURES

This chapter describes the experimental procedures used in obtaining tire pavement contact pressure distributions and lists the experimental parameters which were selected for measurement.

EXPERIMENTAL PARAMETERS

Fuji and ink prints were produced for various combinations of tires, wheel loads, and inflation pressures. The parameters and the reasons for their selection are discussed below. The experimental parameters are tabulated in Table 3.1.

TABLE 3.1. TIRE EXPERIMENTAL PARAMETERS

Tire Type	Inflation Pressure (psi)	Loads (lb)	Inflation Pressure (psi)	Loads (lb)
18-22.5	85	15,000	100	15,000
275/80R/24.5	95	6,000	110	6,000
	95	8,000	110	8,000
255/70R/22.5	110	6,000	135	6,000
	110	8,000	135	8,000
11R24.5	95	6,000	110	6,000
	95	8,000	110	8,000

Tires

Four truck tires were selected for experimentation: a bias Goodyear 18-22.5 LR-H super single tire, a radial Michelin 275/80R/24.5 LR-G tire, a radial Michelin 255/70R22.5 LR-G tire, and a radial Goodyear 11R24.5 LR-G tire. The bias Goodyear 18-22.5 LR-H truck tire, tested by Hansen (Ref 1), was subjected to further tests to obtain more information on this tire, due to its popularity and growing demand.

The radial Michelin 275/80R/24.5 LR-G tire, the radial Michelin 255/70R/22.5 LR-G tire, and the radial Goodyear 11R24.5 LR-G tire were selected due to their popularity on Texas highways. In fact, the radial 11R24.5 tire is generally considered to be the most common truck tire found running on U.S. highways today (Refs 3 and 7).

Loads and Inflation Pressures

All the tires except the bias Goodyear 18-22.5 LR-H super single tire were tested at the maximum inflation pressures and loads recommended by the manufacturers and also at loads and inflation pressures that were roughly 20 percent higher. For the bias Goodyear 18-22.5 tire, it was decided to load the tire at 15,000 pounds under the inflation pressures (85 and 100 psi) used by Hansen (Ref 1). The applied wheel loads and tire inflation pressures are shown in Table 3.1.

EXPERIMENTAL PROCEDURE

The flow chart of the experimental procedure used to obtain tire contact pressure distributions is shown in Fig 3.1. The experimental procedure used in this project consisted of four stages: (1) mounting the tire, (2) testing the tire and producing calibration squares, (3) analysis of the Fuji and ink prints, and (4) presentation of results. For additional details on the experimental procedure, consult Ref 1.

Mounting the Tire

The work prior to the testing consisted of mounting the tire and placing the tire into the load frame, which was followed by operations such as tightening the connections, adjusting the alignment, installing the load calibration cell, and controlling the tire inflation pressure to the desired setting. Figure 3.2 shows the setup for the experiment: the mounted tire ready for testing, the load frame, the hydraulic pumps, the platform, the data acquisition system, and the load cell.

Testing the Tire and Producing Calibration Squares[1]

Fuji and ink prints were made of the tires as they were subjected to different combinations of wheel loads and inflation pressures. The procedure was similar to the one followed by Hansen (Ref 1), except that here the side tire movements were also recorded. This was done by measuring the horizontal and vertical deflections of previously selected reference points (see Appendix B for side tire movement data).

(1) When pressure is applied to a Fuji prescale film, the film changes color in such a way that darker pigmentation is produced in zones of higher pressure. The Fuji or pressure prints are used to relate the contact pressures with color intensities. The Fuji prescale films are comprised of "A" and "C" sheets. Both sheets have a low compressibility polyester base. The A sheet has a thin coating of microcapsule, color-forming material, and the C sheet has a thin coating of color

[1] A special strategy was followed for the bias Goodyear 18-22.5 LR-H tire, since it was felt that in this case the peak pressure values would not be recorded, because they were beyond the capacity (0 to 285 psi) of the Fuji Super Low film. Hansen stated that there was a possibility of not recording higher pressure values due to the limited capacity of the Fuji Super Low film. The very high intensities suggest that pressure values could become as high as 500 psi or even 600 psi. Hence, an additional experiment was conducted using Fuji Low range film, which has a higher capacity (170 to 1,000 psi).

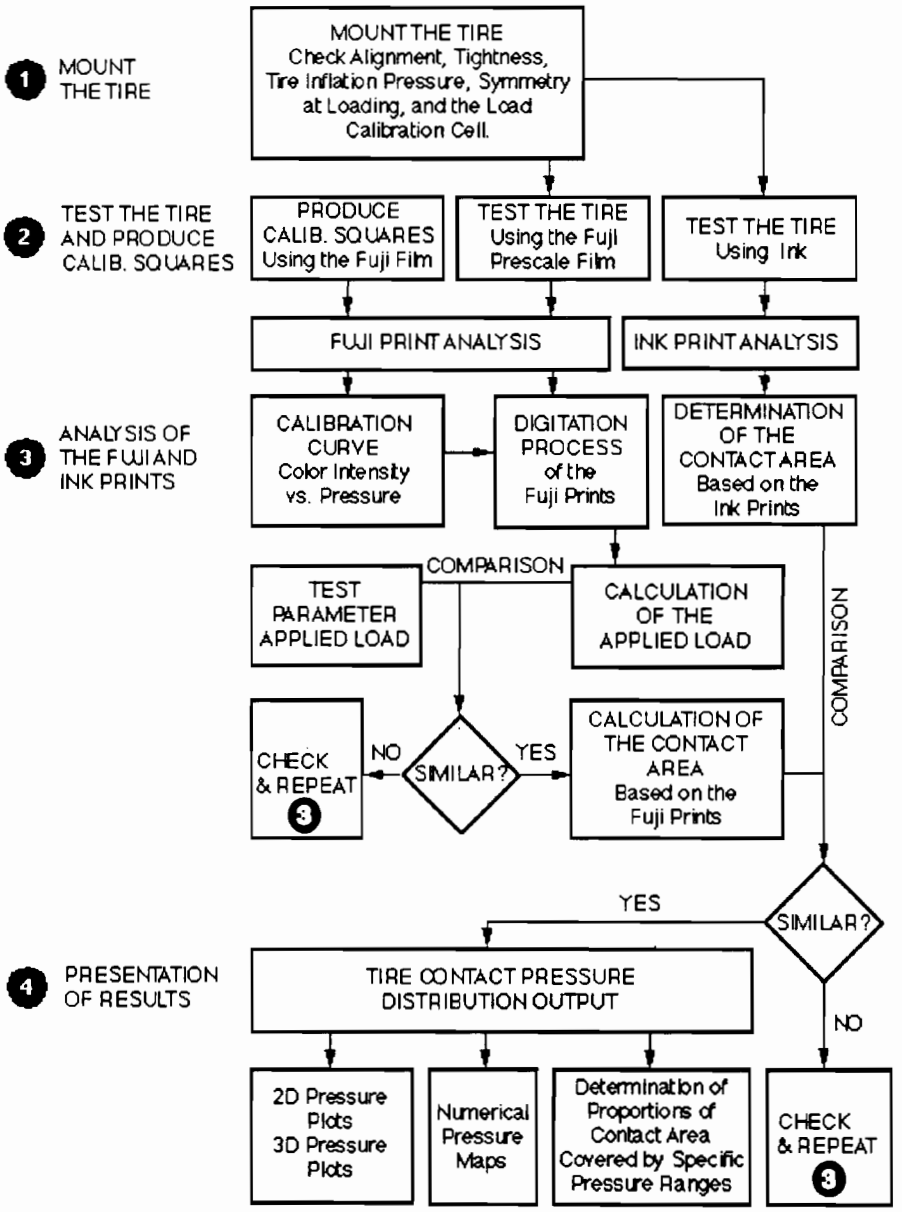

Fig 3.1. Flow chart of the experimental procedures used to obtain tire contact pressure distributions.

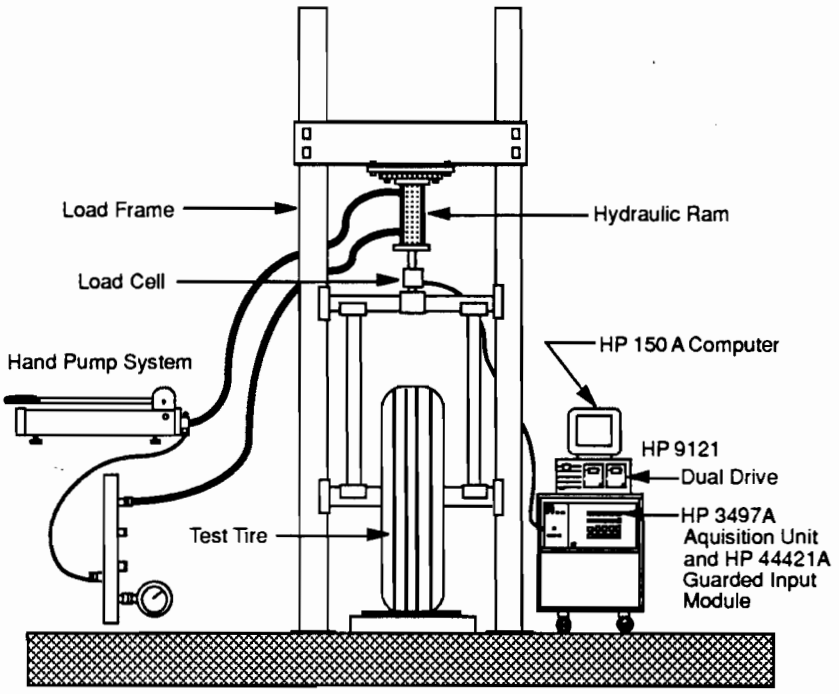

Fig 3.2. Load frame schematic (Ref 1).

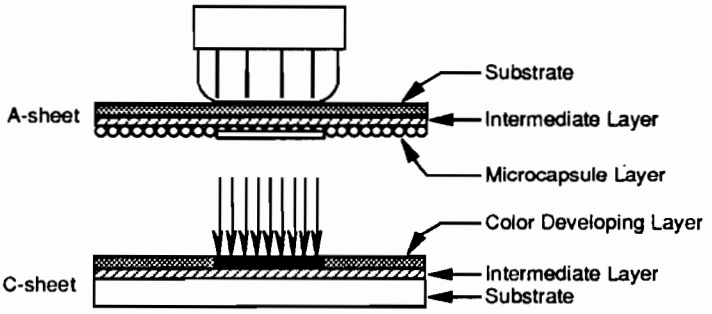

Fig 3.3. Fuji prescale film working principle (Ref 1).

developing material. The microcapsules on the A sheets are of various sizes, and this allows them to break at different pressure levels. Large microcapsules break at relatively low pressures, while smaller capsules break at higher pressures. To produce a color density image, the A and C sheets are superimposed with the coated surfaces face to face. As pressure is applied, the microcapsules on the A sheets break, releasing the color material. Figure 3.3, which is taken from Ref 1, shows the working principle of the Fuji prescale film.

(2) The calibration squares were produced on the Fuji prescale film using a compression machine. These squares were produced at different loads in order to have a variety of points to enable us to analyze and construct a calibration curve to relate color intensities with pressure values. Since

the Fuji prescale film changes with time and from box to box, these calibration squares were produced at approximately the same time as the Fuji prints; and, in the case where two separate boxes of Fuji prescale film were used to complete the testing of one tire, a set of calibration squares was produced for each box of film.

(3) The ink prints were produced under the same testing parameters as the Fuji prints. The monochrome ink prints were used for calculating the tire-plate contact areas. The ink prints were made by applying a common black ink to the tire and pressing the tire down on a white paper that covered the steel plate. From these prints, the tire contact areas were determined using the counting method, i.e., by placing a transparent grid paper on the ink print and counting the number of shaded squares in the transparent grid paper.

(4) The side tire movements were determined by selecting five reference points on the bias Goodyear 18-22.5 LR-H super single tire and four reference points on the other tires. Then the horizontal and vertical deflections of these reference points were measured. These data are recorded in Appendix B.

Analysis of the Fuji and Ink Prints

Analysis of the Fuji prints consisted of running the programs developed by Chan (Ref 2), with some modifications by these authors, and calculating the tire contact areas from the ink prints. The Adage System was used to digitize and analyze the Fuji prints. The Adage system consists of an Eikonix Scanner and an Adage 3006 Graphics System. A tire image analysis program was run on this system to determine the contact pressure distributions. Complete details of the Adage system can be found in Ref 2 and in the Advanced Graphics Laboratory of The University of Texas at Austin. Also, a complete explanation the computer programs used to determine the tire contact pressure distributions can be found in Refs 1 and 2. A brief description of these is included in Appendix A.

During the analysis of the Fuji prints, two checks were performed in order to validate the tire contact pressure distribution output. These checks were done for each tire and at each set of experimental parameters. The first check was to compare the calculated load obtained from the Adage system with the actual wheel load applied during testing. The second check was to compare the calculated tire contact area obtained from the Adage system with the tire contact area obtained from the counting method. In order to have high reliability, these differences had to have an offset of less than 5 percent. Otherwise the whole analysis was checked and repeated.

Presentations of Results

The results consisted of 2D contact pressure plots in color, the numerical pressure maps, and the proportions of the tire contact area at different pressure ranges.

The 2D pressure plots were produced in the Adage system. These pressure plots are color spectra representing the tire contact pressure distributions. These plots are displayed on the screen of the computer monitor and then recorded photographically.

The numerical pressure maps show the actual contact pressure values acting in the contact area. The 2D pressure plots and the numerical pressure maps present the same data but in different ways.

The proportions of the contact area covered by the following pressure ranges were determined from the numerical pressure maps: (1) <50 psi, (2) 50 to 100 psi, (3) 101 to 150 psi, (4) 151 to 200 psi, (5) 201 to 250 psi, (6) 251 to 300 psi, and (7) >300 psi. This was done to provide more information on the tire-pavement contact pressure distributions.

For the bias Goodyear 18-22.5 LR-H tire, results from both the Fuji Super Low and the Fuji Low range films were combined, and the proportions of contact areas for the following pressure ranges were determined: 301 to 400 psi, 401 to 500 psi, 501 to 600 psi, and >600 psi.

CHAPTER 4. EXPERIMENTAL RESULTS

Using the Fuji prescale film and the Adage analysis system, contact pressure distributions for the bias Goodyear 18-22.5 LR-H "Super Single" tire, the radial Michelin 275/80R/24.5 LR-G tire, the radial Michelin 255/70R22.5 LR-G tire, and the radial Goodyear 11R24.5 LR-G tire were recorded and analyzed. The experimental parameters and the resulting contact pressures for each tire are presented.

BIAS GOODYEAR 18-22.5 LR-H "SUPER SINGLE" TIRE

The bias Goodyear 18-22.5 LR-H truck tire, tested by Hansen (Ref 1), was subjected to further tests to obtain more information on this tire, due to its popularity and growing demand. Hansen (Ref 1) tested this tire at 8,000, 10,000, and 12,000 pounds, at inflation pressures of 85 and 100 psi. Here, this tire was tested at 15,000 pounds, at the same inflation pressures. Both films, the Super Low and the Low range Fuji prescale films, were used. Also, ink prints were produced in each case.

Table 4.1 shows (1) the print width, (2) the print length, (3) the mean contact pressure values, (4) the tire contact area obtained from the Adage system, and (5) the tire contact area obtained from the counting method for the various tire inflation pressures and wheel loads. Note that, in general, the mean contact pressures are higher than the tire inflation pressures. The differences in the tire contact areas obtained from the Adage system and the counting method are on the order of ± 5 percent. For this tire, results from the Fuji "Super Low" and the Fuji "Low" range films were combined. Table 4.2 shows the contact area for various pressure ranges for the case where the wheel load is 15,000 pounds.

The contact areas covered by the various pressure ranges are computed from the numerical pressure maps presented by Hansen (Ref 1) for the 12,000, 10,000, and 8,000-pound wheel load cases. These data are tabulated in Table 4.3. Table 4.4 shows the load distribution across the tread width, obtained from the Adage system, when the tire was tested at the 15,000-pound wheel load.

Figures 4.1 and 4.2 show two-dimensional contact pressure plots in color for the tire loaded to a 15,000-pound load when inflated to 100 and 85 psi, respectively. Figures 4.3 and 4.4 show the numerical contact pressure maps for the same parameters. Figures 4.5 through 4.10 have been constructed using the data from Tables 4.2 and 4.3. These histograms show the effects of changing from one load to another load, and from one inflation pressure to another inflation pressure.

RADIAL MICHELIN 275/80R/24.5 LR-G TIRE

The radial Michelin 275/80R/24.5 LR-G tire was analyzed following the same procedure described in Chapter 3. This tire was tested under its rated parameters and under a set of parameters roughly 20 percent higher. This tire is rated for a maximum load of 6,005 pounds and a maximum inflation pressure of 100 psi. This tire was tested at 6,000 and 8,000 pounds, at inflation pressures of 95 and 110 psi. Ink prints were produced in each case.

The tire contact areas obtained from the Adage system and the counting method, the print width and print length of the contact areas, and the mean contact pressures are tabulated in Table 4.5. Note that, in general, the mean contact pressures are higher than the tire inflation pressures. The differences in the tire contact areas obtained from the Adage system and the counting method are on the order of ± 5 percent.

The proportions of contact area covered by the various pressure ranges are computed from the numerical pressure

TABLE 4.1. BIAS GOODYEAR 18-22.5 TIRE TEST DIMENSIONS

Inflation Pressure (psi)	Wheel Load (lb)	Print Width (in.)	Print Length (in.)	Mean Contact Pressure (psi)	Tire Contact Area	
					Adage (sq in.)	Manual (sq in.)
85	8,000	11.9	11.5	99.40	75.60	80.48
85	10,000	12.1	12.8	105.57	99.90	94.72
85	12,000	12.4	13.8	109.04	114.94	110.05
85	15,000	12.4	15.2	108.95	122.04	126.10
100	8,000	11.4	11.1	102.15	74.40	78.32
100	10,000	12.1	12.1	110.74	87.70	90.30
100	12,000	12.4	12.3	111.80	112.04	107.33
100	15,000	12.4	14.3	124.79	116.26	120.20

TABLE 4.2. BIAS 18-22.5 PROPORTIONS OF CONTACT AREA (PERCENT) FOR THE 15,000-POUND WHEEL LOAD

Pressure Ranges (psi)	Inflation Pressure	
	85 psi	100 psi
< 50	3.43	0.23
50-100	36.00	36.50
101-150	28.51	25.67
151-200	22.25	23.91
201-250	6.87	10.68
251-300	1.08	1.23
301-400	1.05	1.10
401-500	0.52	0.44
501-600	0.17	0.15
> 600	0.12	0.09

TABLE 4.3. BIAS 18-22.5 PROPORTIONS CONTACT AREA (PERCENT) OF THE 12,000, 10,000, AND 8,000-POUND WHEEL LOADS

Pressure Ranges (psi)	12,000-lb Load		10,000-lb Load		8,000-lb Load	
	Inflation Pressure					
	85 psi	100 psi	85 psi	100 psi	85 psi	100 psi
< 50	0.73	0.71	3.45	9.02	6.35	7.01
50-100	54.68	53.08	61.69	46.90	54.26	48.65
101-150	27.12	28.23	25.49	24.39	28.49	28.56
151-200	13.05	13.61	4.70	12.13	5.96	9.35
201-250	3.28	3.37	2.28	4.36	2.83	3.66
251-300	1.14	1.00	1.23	2.20	1.43	1.90
>300	0.00	0.00	1.16	1.00	0.68	0.87

TABLE 4.4. BIAS 18-22.5 LOAD DISTRIBUTION (LB) ACROSS THE TREAD WIDTH FOR THE 15,000-POUND LOAD

Position Tread Width	Inflation Pressure	
	85 psi	100 psi
Left	2339.3	2237.8
Left-Center	3249.1	3303.6
Center	3363.7	3569.5
Right-Center	3244.1	3370.4
Right	2803.3	2518.7

maps for the 6,000 and 8,000-pound wheel load cases. These data are tabulated in Table 4.6. Table 4.7 shows the load distribution across the tread width, obtained from the Adage system, when the tire was tested at the tire inflation pressures and wheel loads given in Table 3.1.

Figures 4.11 and 4.12 show two-dimensional contact pressure plots for the tire loaded to a 6,000-pound load when inflated to 95 and 110 psi, respectively. Figures 4.13 and 4.14 show two-dimensional contact pressure plots for the tire loaded to an 8,000-pound load when inflated to 95 and 110 psi, respectively. Figures 4.15 through 4.18 show the numerical contact pressure maps for the same parameters. Figures 4.19 through 4.22 have been constructed using the data from Table 4.6. These histograms show the effects of changing from one load to another load, and from one inflation pressure to another inflation pressure.

RADIAL MICHELIN 255/70R/22.5 LR-G TIRE

The radial Michelin 255/70R/22.5 LR-G tire was analyzed following the procedure described in Chapter 3. This tire was tested under its rated parameters and under a set of parameters roughly 20 percent higher. This tire is rated for a maximum load of 5,510 pounds and a maximum inflation pressure of 115 psi. This tire was tested at 6,000 and 8,000 pounds, at inflation pressures of 110 and 135 psi. Ink prints were produced in each case.

The tire contact areas obtained from the Adage system and the counting method, the print width and print length of the contact areas, and the mean contact pressures are tabulated in Tables 4.8. Note that, in general, the mean contact pressures are higher than the tire inflation pressures. The differences in the tire contact areas obtained from the Adage system and the counting method are on the order of ± 5 percent.

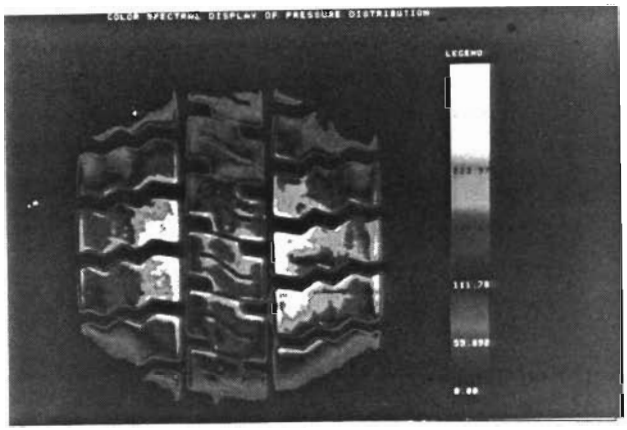

Fig 4.1. Two-dimensional contact pressure plot for the bias Goodyear 18-22.5 LR-H tire inflated to 100 psi and loaded to 15,000 pounds.

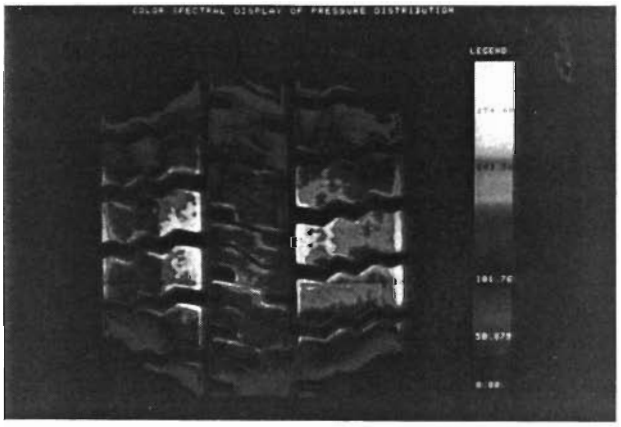

Fig 4.2. Two-dimensional contact pressure plot for the bias Goodyear 18-22.5 LR-H tire inflated to 85 psi and loaded to 15,000 pounds.

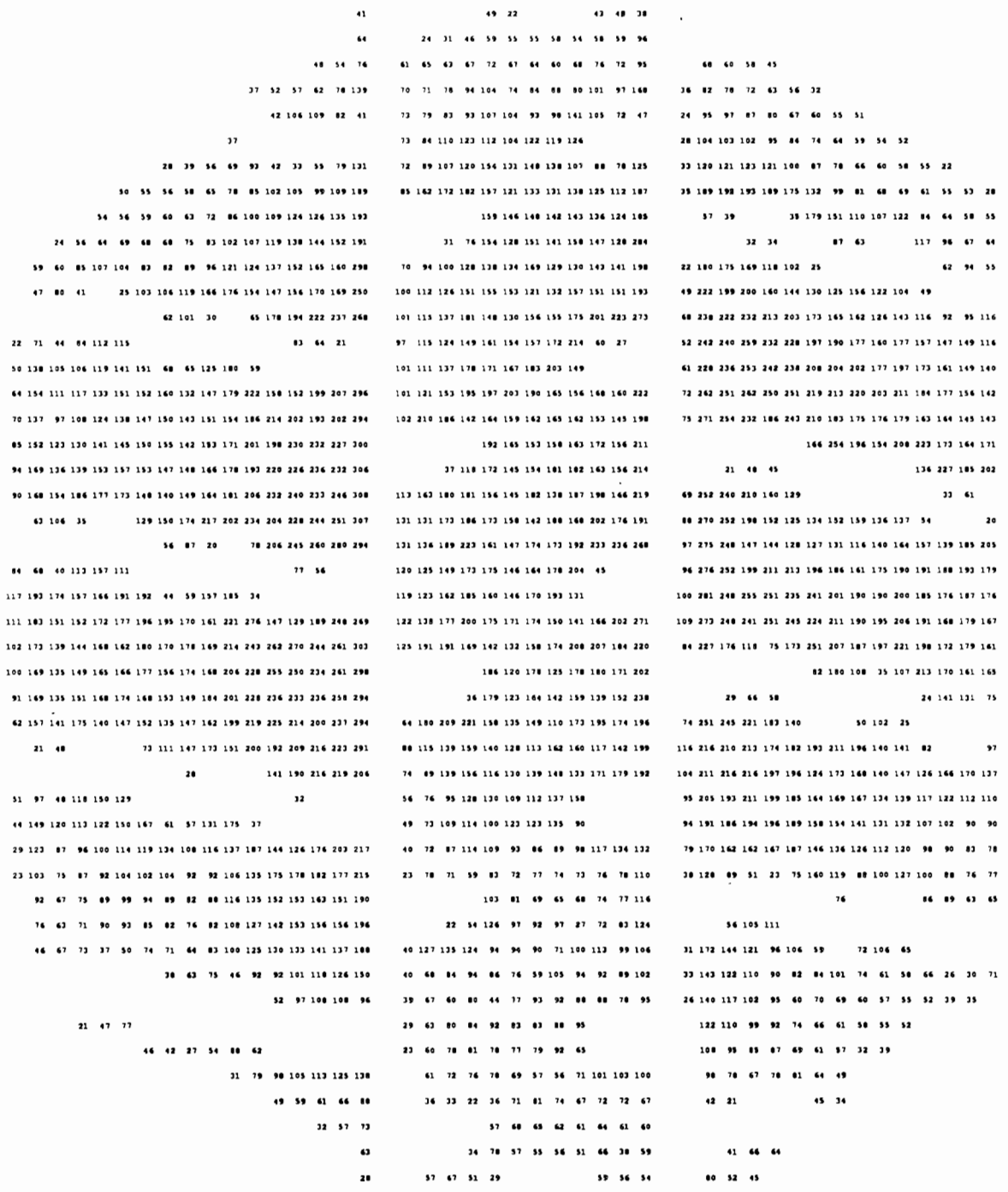

Fig 4.3. Numerical pressure map for the bias Goodyear 18-22.5 LR-H tire inflated to 100 psi and loaded to 15,000 pounds. The pressure print is 14.3 inches long and 12.4 inches wide.

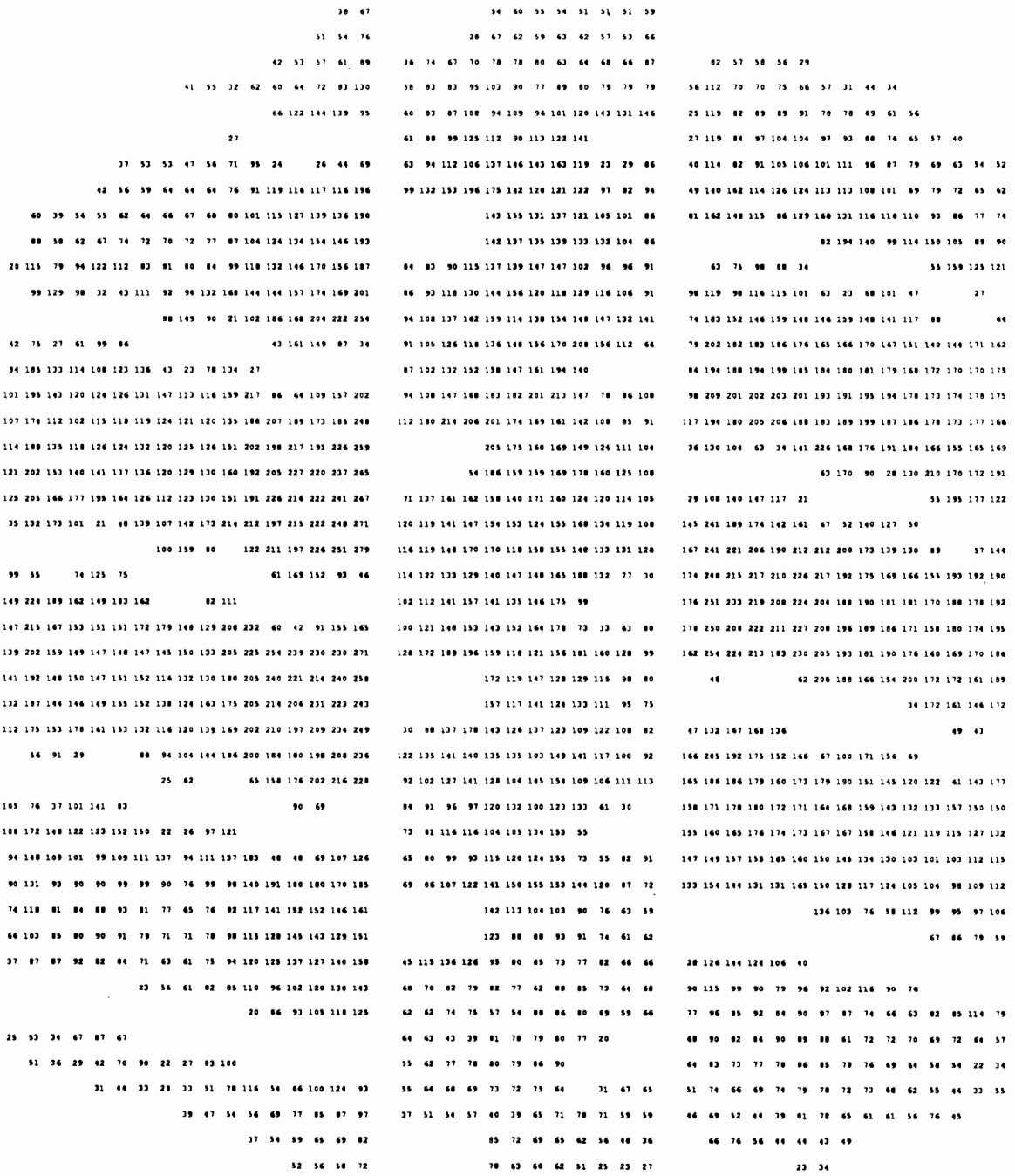

Fig 4.4. Numerical pressure map for the bias Goodyear 18-22.5 LR-H tire inflated to 85 psi and loaded to 15,000 pounds. The pressure print is 14.3 inches long and 12.4 inches wide.

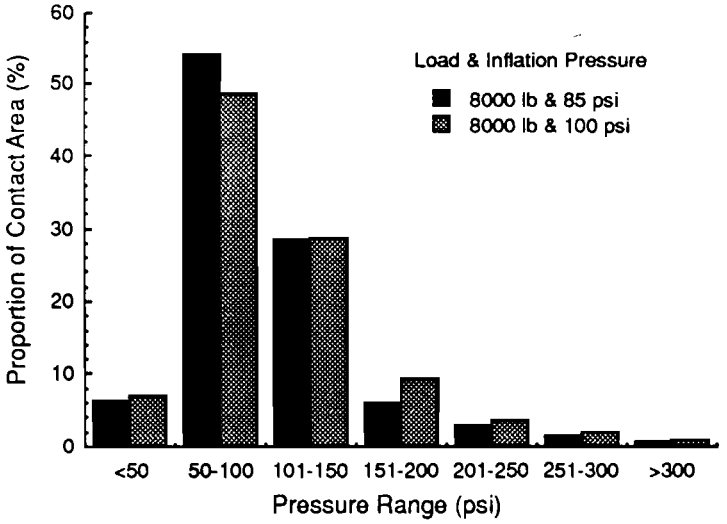

Fig 4.5. Histogram for the bias Goodyear 18-22.5 LR-H tire. Shown are the proportions of contact area at the various contact pressure ranges for a 8,000-pound wheel load and inflation pressures of 85 and 100 psi.

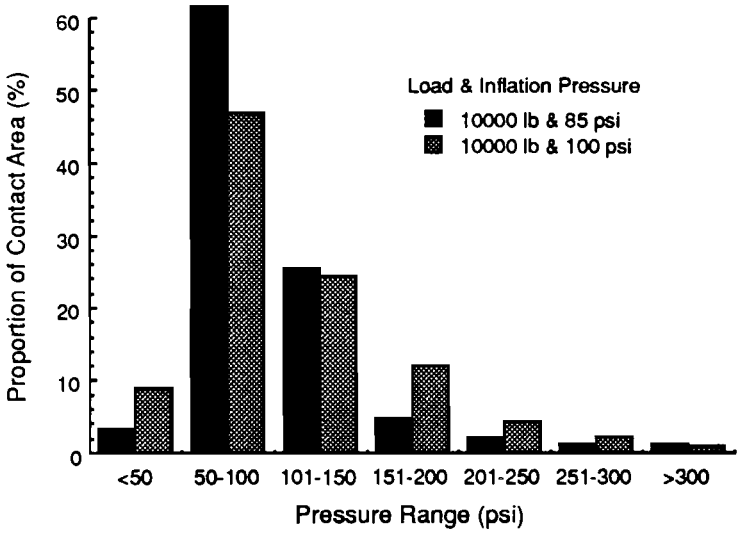

Fig 4.6. Histogram for the bias Goodyear 18-22.5 LR-H tire. Shown are the proportions of contact area at the various contact pressure ranges for a 10,000-pound wheel load and inflation pressures of 85 and 100 psi.

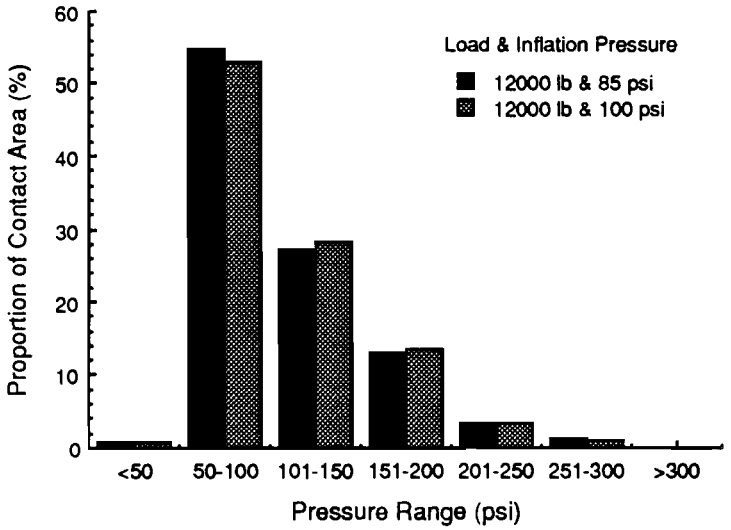

Fig 4.7. Histogram for the bias Goodyear 18-22.5 LR-H tire. Shown are the proportions of contact area at the various contact pressure ranges for a 12,000-pound wheel load and inflation pressures of 85 and 100 psi.

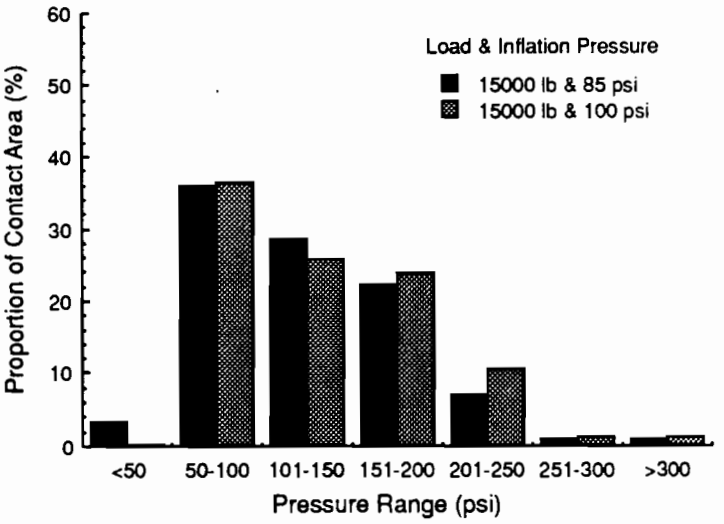

Fig 4.8. Histogram for the bias Goodyear 18-22.5 LR-H tire. Shown are the proportions of contact area at the various contact pressure ranges for a 15,000-pound wheel load and inflation pressures of 85 and 100 psi.

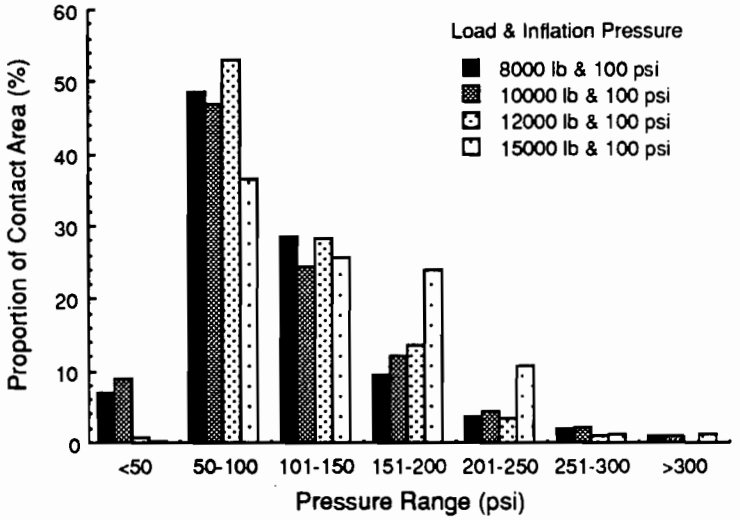

Fig 4.9. Histogram for the bias Goodyear 18-22.5 LR-H tire. Shown are the proportions of contact area at the various contact pressure ranges for an inflation pressure of 100 psi and loads of 8,000, 10,000, 12,000 and 15,000 pounds.

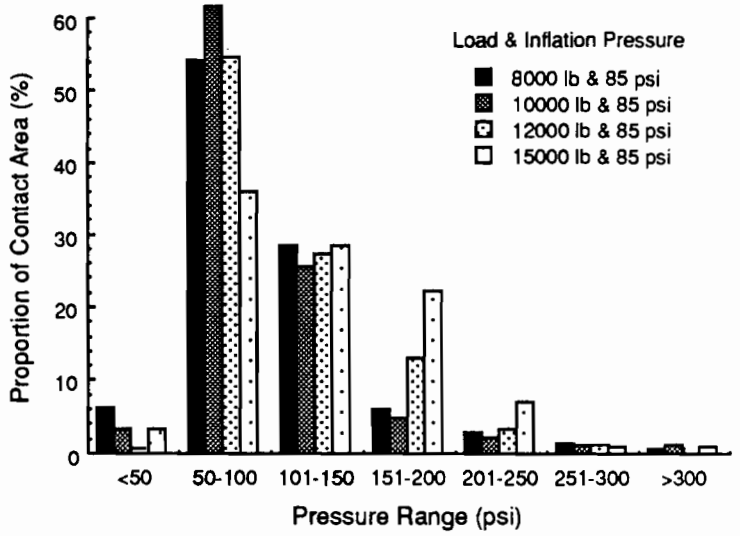

Fig 4.10. Histogram for the bias Goodyear 18-22.5 LR-H tire. Shown are the proportions of contact area at the various contact pressure ranges for an inflation pressure of 85 psi and loads of 8,000, 10,000, 12,000 and 15,000 pounds.

The proportions of contact area covered by the various pressure ranges are computed from the numerical pressure maps for the 6,000 and 8,000-pound wheel load cases. These data are tabulated in Table 4.9. Table 4.10 shows the load distribution across the tread width, obtained from the Adage system, when the tire was tested at these experimental parameters.

Figures 4.11 and 4.12 show two-dimensional contact pressure plots for the tire loaded to a 6,000-pound load when inflated to 95 and 110 psi, respectively. Figures 4.13 and 4.14 show two-dimensional contact pressure plots for the tire loaded to an 8,000-pound load when inflated to 95 and 110 psi, respectively. Figures 4.15 through 4.18 show the numerical contact pressure maps for the same parameters. Figures 4.19 through 4.22 have been constructed using the data from Table 4.6. These histograms show the effects of changing from one load to another load and from one inflation pressure to another inflation pressure.

TABLE 4.5. RADIAL 275/80R/24.5 TIRE TEST DIMENSIONS

Inflation Pressure (psi)	Wheel Load (lb)	Print Width (in.)	Print Length (in.)	Mean Contact (psi)	Tire Contact Area	
					Adage (sq in.)	Manual (sq in.)
95	6,000	7.28	10.16	113.87	54.60	52.69
95	8,000	7.28	11.81	125.90	62.70	63.54
110	6,000	7.28	10.16	123.18	51.20	48.71
110	8,000	7.28	11.85	140.35	61.27	57.00

TABLE 4.6. RADIAL MICHELIN 275/80R/24.5 PROPORTIONS OF CONTACT AREA (PERCENT) FOR THE 6,000 AND 8,000 POUNDS

Pressure Ranges (psi)	6,000-lb Load		8,000-lb Load	
	Inflation Pressure			
	95 psi	110 psi	95 psi	110 psi
< 50	3.94	3.83	3.45	1.81
50-100	44.14	37.85	37.93	33.90
101-150	28.47	32.42	27.13	31.22
151-200	16.32	20.21	17.67	17.92
201-250	6.68	5.45	10.60	12.53
251-300	0.45	0.18	3.04	2.60
>300	0	0	0.18	0.02

RADIAL GOODYEAR 11R24.5 LR-G TIRE

The radial Goodyear 11R24.5 LR-G was analyzed following the same procedure described in Chapter 3. This tire was tested under its rated parameters and under a set of parameters roughly 20 percent higher. This tire is rated for a maximum load of 6,430 pounds and a maximum inflation pressure of 105 psi. This tire was tested at 6,000 and 8,000 pounds, at inflation pressures of 95 and 110 psi. Ink prints were produced in each case.

The tire contact areas obtained from the Adage system and the counting method; the print width and print length of the contact areas; and the mean contact pressures are tabulated in Table 4.11. Note that, in general, the mean contact pressures are higher than the tire inflation pressures. The differences in the tire contact areas obtained from the Adage system and the counting method are on the order of ± 5 percent.

The proportions of contact area covered by the various pressure ranges are computed from the numerical pressure maps for the 6,000 and 8,000-pound wheel load cases. These data are tabulated in Table 4.12. Table 4.13 shows the load distribution across the tread width, obtained from the Adage system, when the tire was tested at these experimental parameters.

Figures 4.35 and 4.36 show two-dimensional contact pressure plots for the tire loaded to a 6,000-pound load when inflated to 95 and 110 psi, respectively. Figures 4.37 and 4.38 show two-dimensional contact pressure plots for the tire loaded to an 8,000-pound load when inflated to 95 and 110 psi, respectively. Figures 4.39 through 4.42 show the numerical contact pressure maps for the same parameters. Figures 4.43 through 4.46 have been constructed using the data from Tables 4.6. These histograms show the effects of changing from one load to another load, and from one inflation pressure to another inflation pressure.

TABLE 4.7. RADIAL MICHELIN 275/80R/24.5 LOAD DISTRIBUTION (LB) ACROSS THE TREAD WIDTH FOR 6,000 AND 8,000 POUNDS

Position Tread Width	6,000-lb Load		8,000-lb Load	
	Inflation Pressure			
	95 psi	110 psi	95 psi	110 psi
Left	1241.4	1189.4	1748.8	1790.6
Left-Center	1081.2	1133.4	1285.3	1429.9
Center	1241.3	1361.5	1565.6	1639.2
Right-Center	1084.1	1107.2	1497.5	1340.6
Right	1352.0	1208.5	1902.8	1799.7

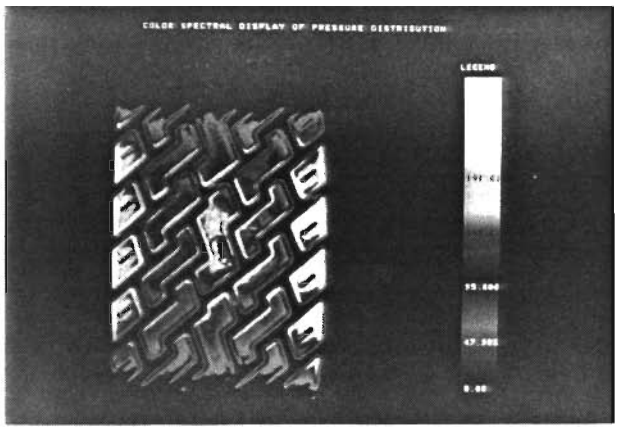

Fig 4.11. Two-dimensional contact pressure plot for the radial Michelin 275/80R/24.5 LR-G tire inflated to 95 psi and loaded to 6,000 pounds.

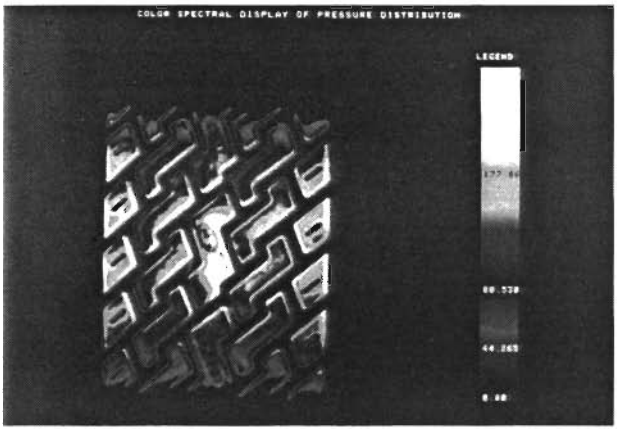

Fig 4.12. Two-dimensional contact pressure plot for the radial Michelin 275/80R/24.5 LR-G tire inflated to 110 psi and loaded to 6,000 pounds.

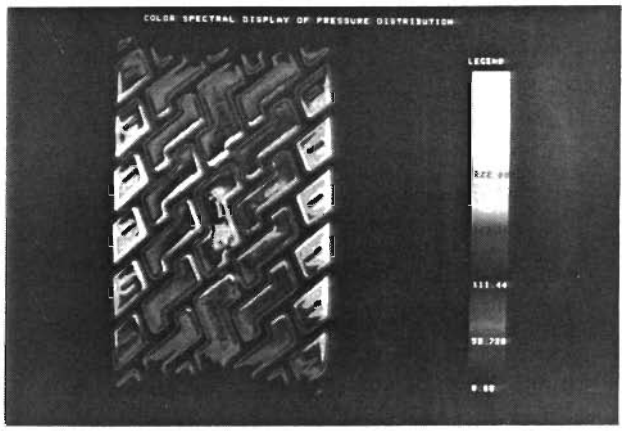

Fig 4.13. Two-dimensional contact pressure plot for the radial Michelin 275/80R/24.5 LR-G tire inflated to 95 psi and loaded to 8,000 pounds.

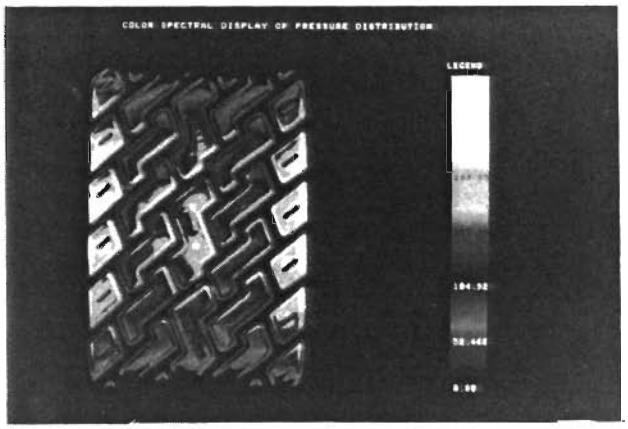

Fig 4.14. Two-dimensional contact pressure plot for the radial Michelin 275/80R/24.5 LR-G tire inflated to 110 psi and loaded to 8,000 pounds.

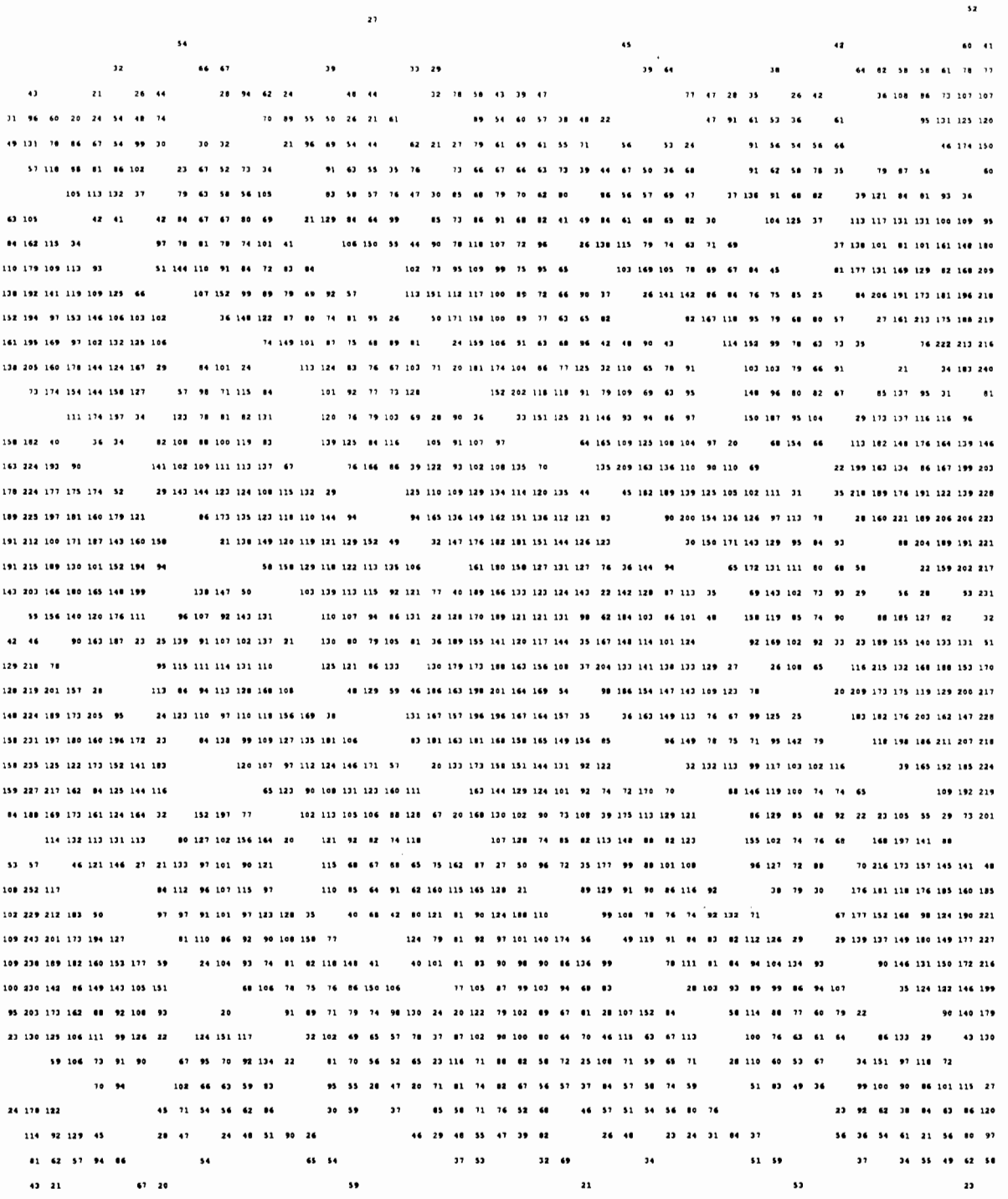

Fig 4.15. Numerical pressure map for the radial Michelin 275/80R/24.5 tire inflated to 95 psi and loaded to 6,000 pounds. The pressure print is 10.16 inches long and 7.28 inches wide.

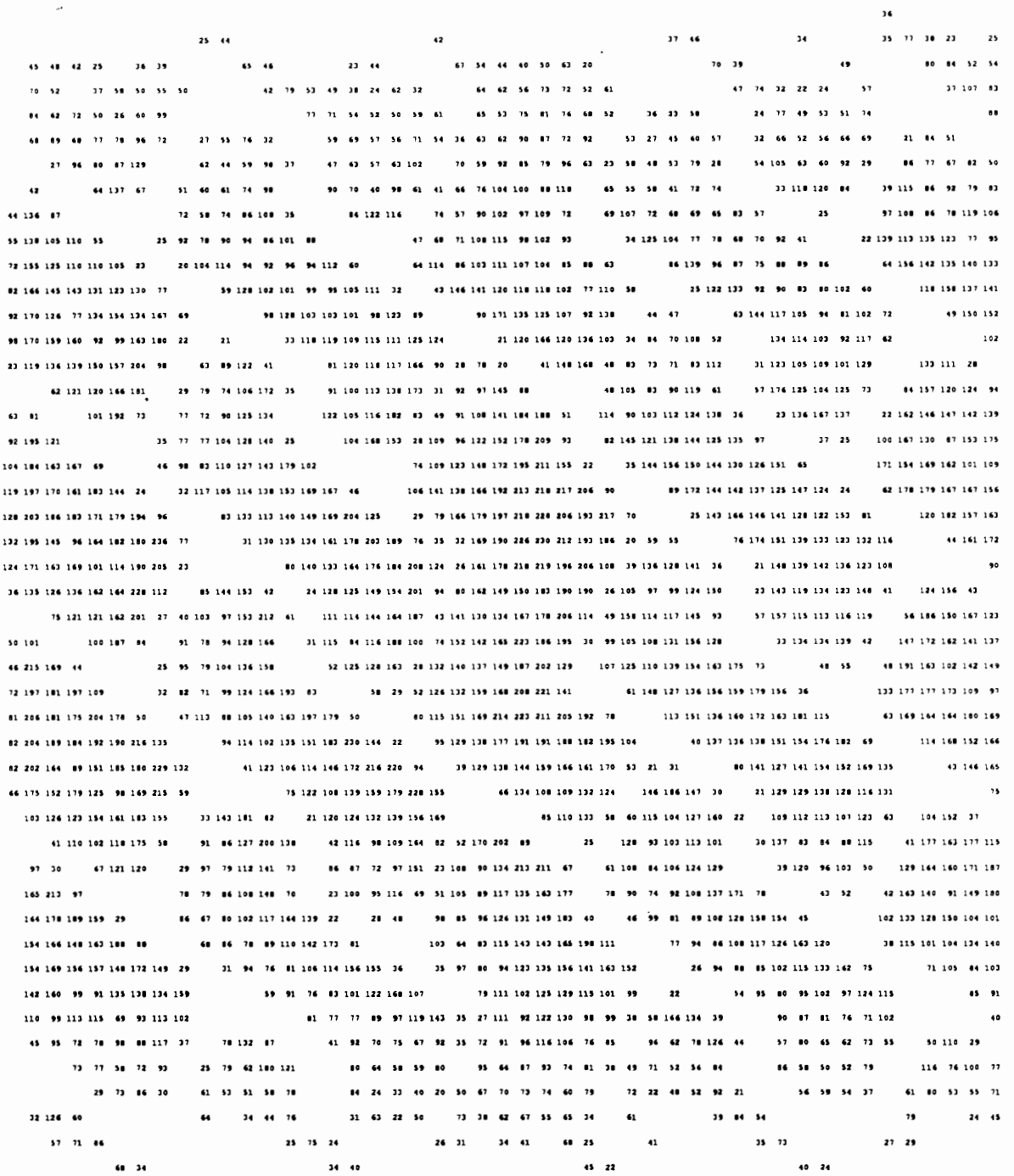

Fig 4.16. Numerical pressure map for the radial Michelin 275/80R/24.5 tire inflated to 110 psi and loaded to 6,000 pounds. The pressure print is 9.65 inches long and 7.28 inches wide.

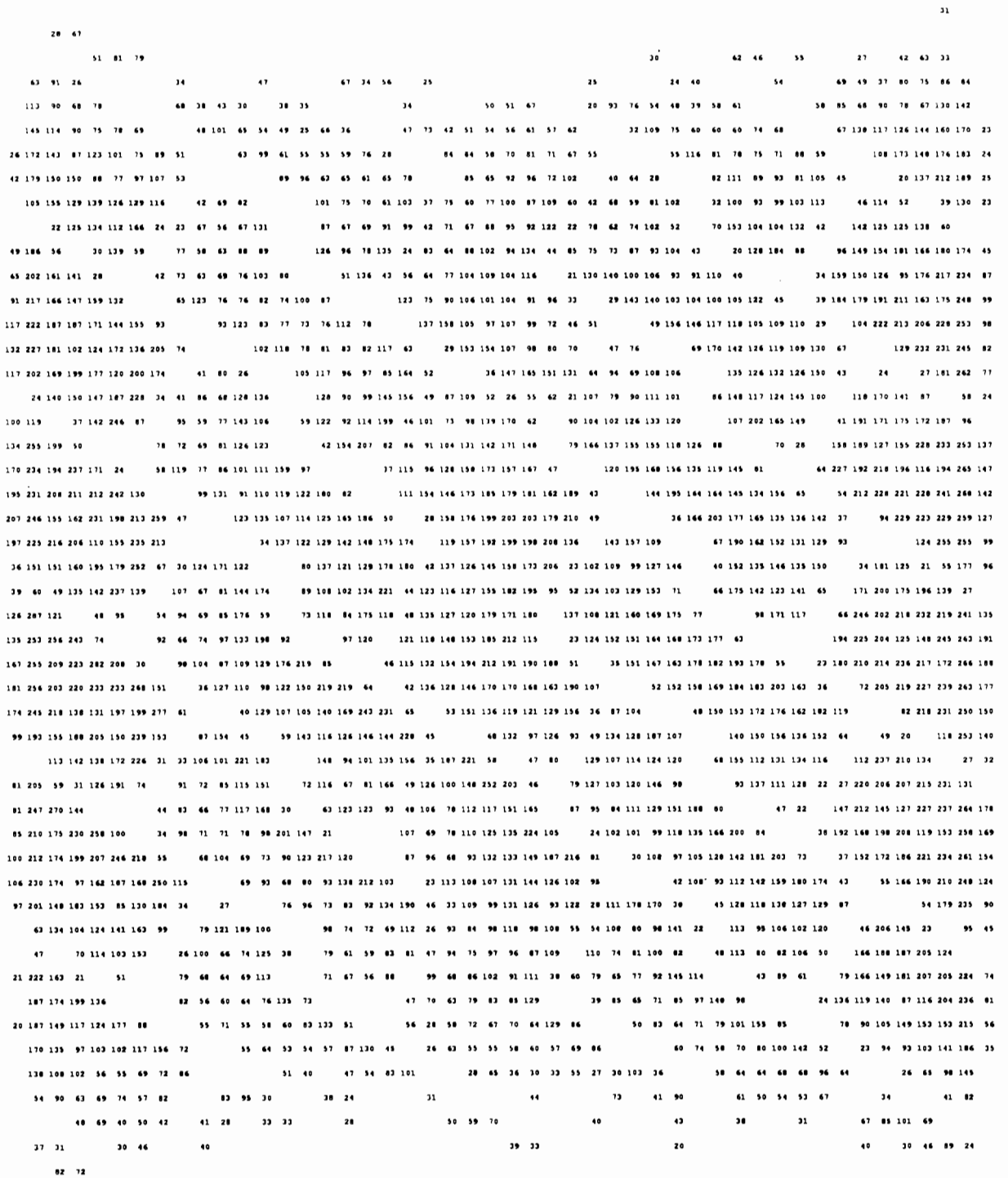

Fig 4.17. Numerical pressure map for the radial Michelin 275/80R/24.5 tire inflated to 95 psi and loaded to 8,000 pounds. The pressure print is 11.81 inches long and 7.28 inches wide.

Fig 4.18. Numerical pressure map for the radial Michelin 275/80R/24.5 tire inflated to 110 psi and loaded to 8,000 pounds. The pressure print is 11.22 inches long and 7.28 inches wide.

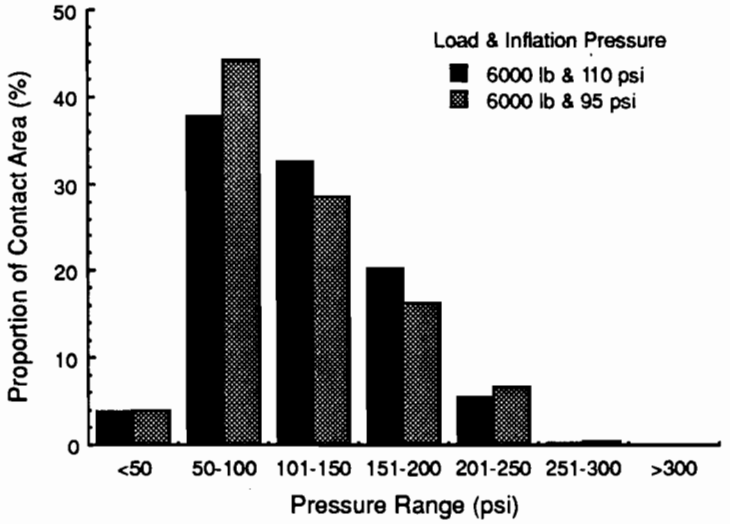

Fig 4.19. Histogram for the radial Michelin 275/80R/24.5 tire. Shown are the proportions of contact area at the various contact pressure ranges at a 6,000-pound wheel load and inflation pressures of 95 and 110 psi.

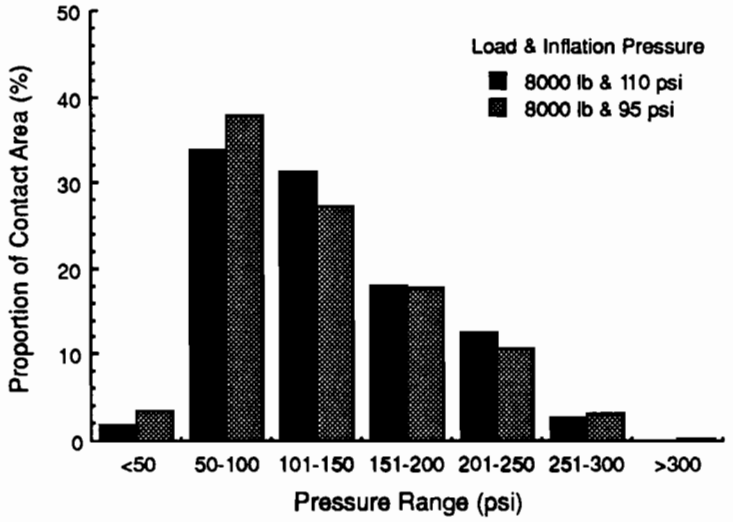

Fig 4.20. Histogram for the radial Michelin 275/80R/24.5 tire. Shown are the proportions of contact area at the various contact pressure ranges for a 8,000-pound wheel load and inflation pressures of 95 and 110 psi.

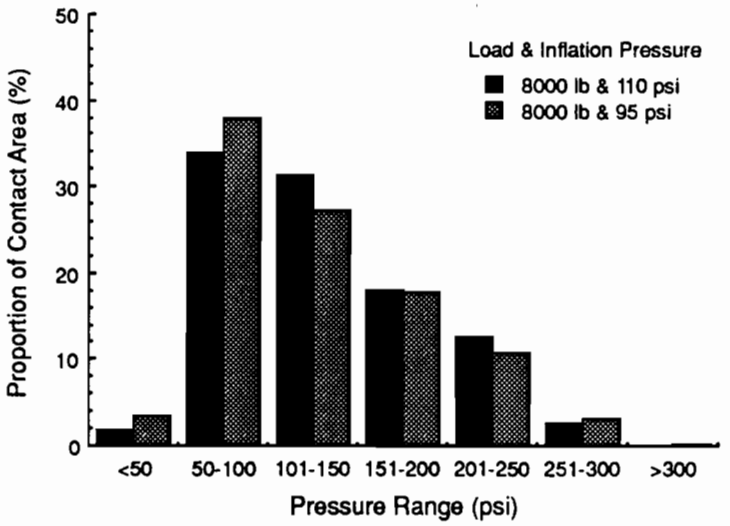

Fig 4.21. Histogram for the radial Michelin 275/80R/24.5 tire. Shown are the proportions of contact area at the various contact pressure ranges for an inflation pressure of 95 psi and wheel loads of 6,000 and 8,000 pounds.

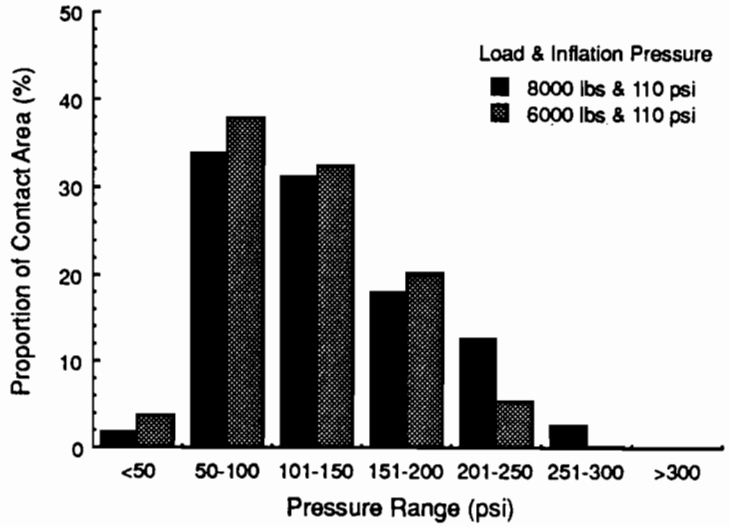

Fig 4.22. Histogram for the radial Michelin 275/80R/24.5 tire. Shown are the proportions of contact area at the various contact pressure ranges for an inflation pressure of 110 psi and wheel loads of 6,000 and 8,000 pounds.

TABLE 4.8. RADIALMICHELLIN 255/70R/22.5 TIRE TEST DIMENSIONS

Inflation Pressure (psi)	Wheel Load (lb)	Print Width (in.)	Print Length (in.)	Mean Contact Pressure (psi)	Tire Contact Area	
					Adage (sq in.)	Manual (sq in.)
110	6,000	7.91	8.27	119.78	48.40	50.09
110	8,000	7.91	9.69	132.00	57.35	60.61
135	6,000	7.91	7.56	132.60	43.73	45.25
135	8,000	7.91	8.74	140.87	54.16	56.79

TABLE 4.9. RADIAL MICHELLIN 255/70R/22.5 PROPORTIONS OF CONTACT AREA (PERCENT) FOR 6,000 AND 8,000 POUNDS

Pressure Ranges (psi)	6,000-lb Load		8,000-lb Load	
	Inflation Pressure			
	110 psi	135 psi	110 psi	135 psi
< 50	8.39	7.45	5.79	5.52
50-100	20.90	19.21	14.86	13.98
101-150	37.71	25.98	25.52	22.21
151-200	32.66	35.35	53.60	46.49
201-250	0.34	12.01	0.23	11.80
251-300	0.00	0.00	0.00	0.00
>300	0.00	0.00	0.00	0.00

TABLE 4.10. RADIAL MICHELLIN 255/70R/22.5 LOAD DISTRIBUTION (LB) ACROSS THE TREAD WIDTH FOR 6,000 AND 8,000 POUNDS

Position Tread Width	6,000-lb Load		8,000-lb Load	
	Inflation Pressure			
	110 psi	135 psi	110 psi	135 psi
Left	1236.1	1074.5	1897.9	1682.1
Left-Center	1176.5	1235.5	1435.5	1488.9
Center	1087.0	1173.7	1290.5	1420.0
Right-Center	1119.8	1329.0	1393.3	1445.6
Right	1380.7	1187.4	1982.7	1963.4

TABLE 4.11. RADIAL 11R24.5 TIRE TEST DIMENSIONS

Inflation Pressure (psi)	Wheel Load (lb)	Print Width (in.)	Print Length (in.)	Mean Contact Pressure (psi)	Tire Contact Area	
					Adage (sq in.)	Manual (sq in.)
95	6,000	7.48	9.65	95.36	66.39	62.92
95	8,000	7.48	11.14	107.86	70.72	74.17
110	6,000	7.48	9.21	103.23	61.05	58.12
110	8,000	7.48	10.63	111.50	73.69	71.75

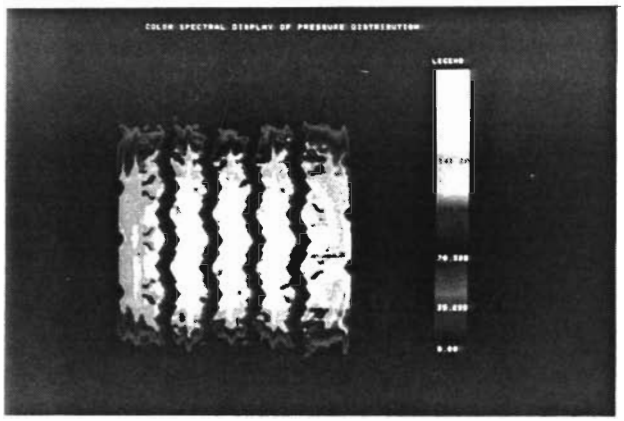

Fig 4.23. Two-dimensional contact pressure plot for the radial Michelin 255/70R/22.5 LR-G tire inflated to 110 psi and loaded to 6,000 pounds.

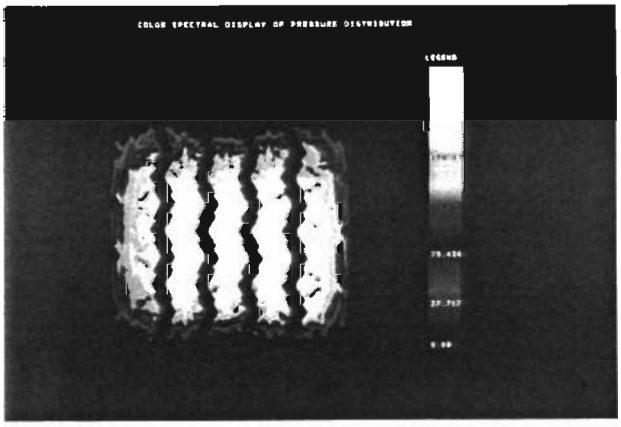

Fig 4.24. T wo-dimensional contact pressure plot for the radial Michelin 255/70R/22.5 LR-G tire inflated to 135 psi and loaded to 6,000 pounds.

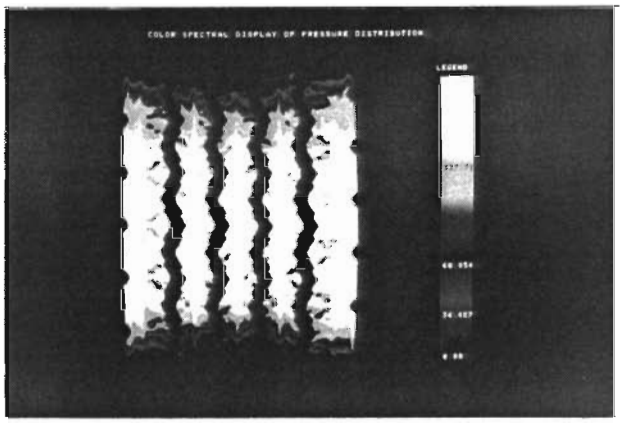

Fig 4.25. T wo-dimensional contact pressure plot for the radial Michelin 255/70R/22.5 LR-G tire inflated to 110 psi and loaded to 8,000 pounds.

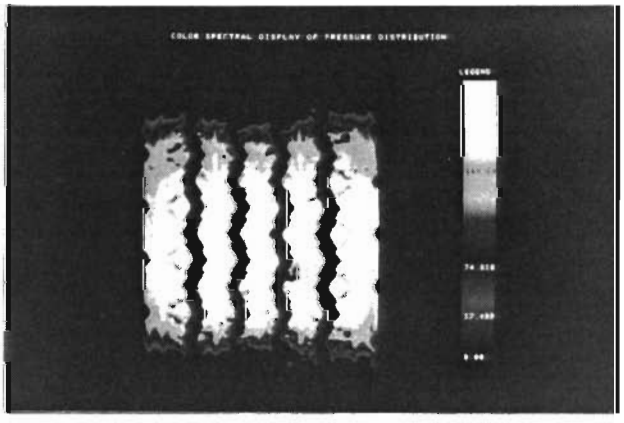

Fig 4.26. T wo-dimensional contact pressure plot for the radial Michelin 255/70R/22.5 LR-G tire inflated to 135 psi and loaded to 8,000 pounds.

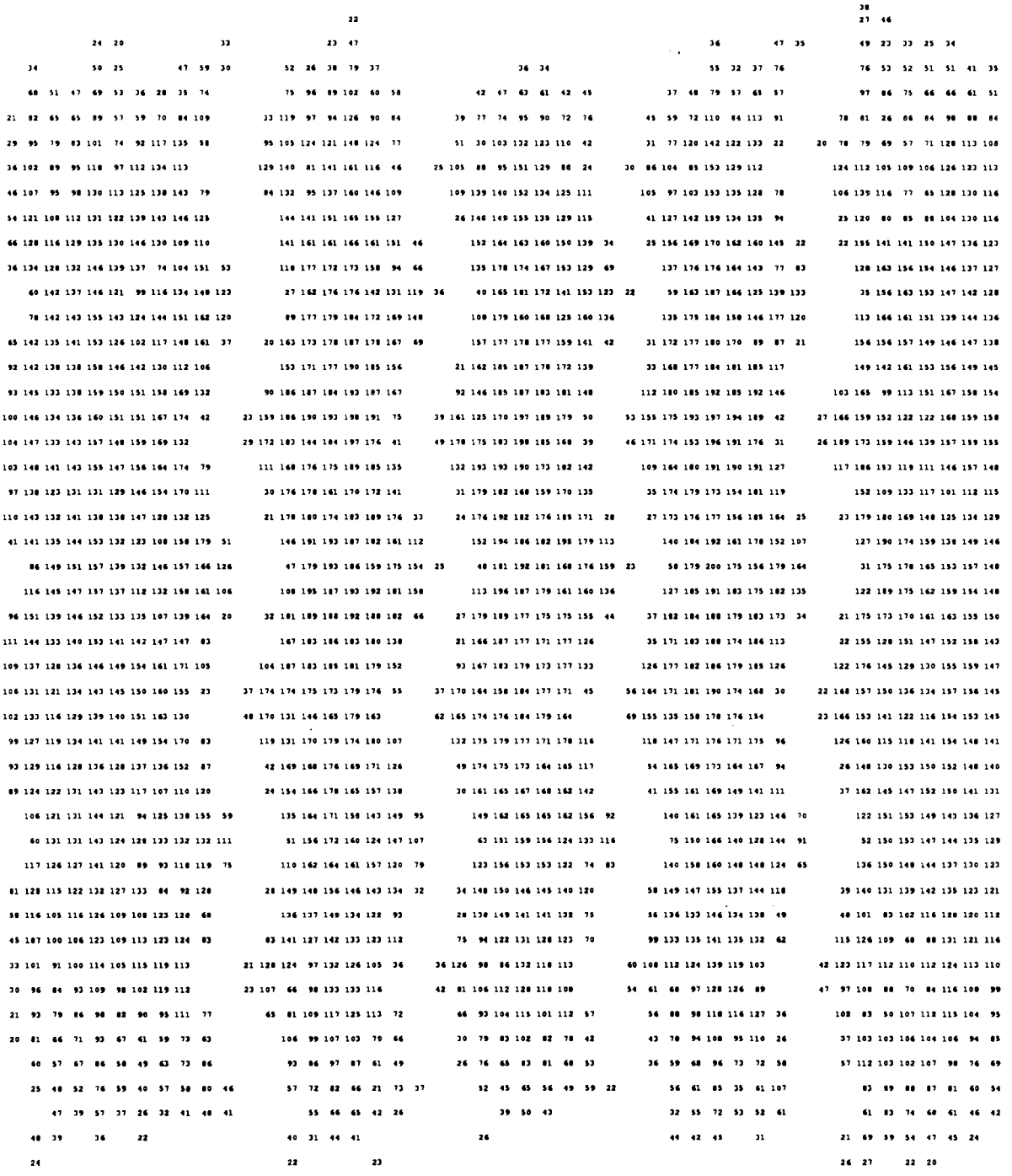

Fig 4.27. Numerical pressure map for the radial Michelin 255/70R/22.5 tire inflated to 110 psi and loaded to 6,000 pounds. The pressure print is 8.27 inches long and 7.91 inches wide.

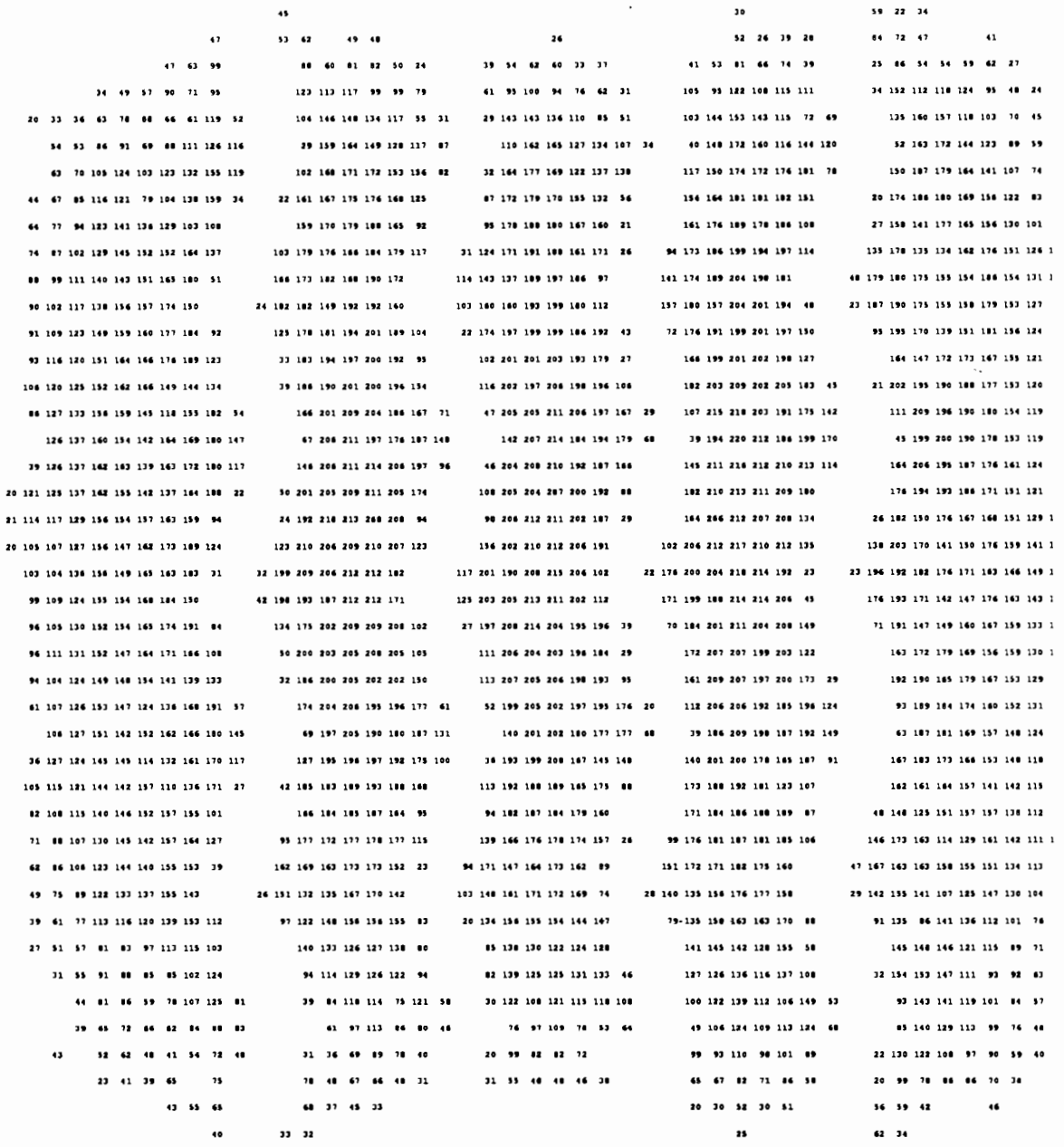

Fig 4.28. Numerical pressure map for the radial Michelin 255/70R/22.5 tire inflated to 135 psi and loaded to 6,000 pounds. The pressure print is 7.56 inches long and 7.91 inches wide.

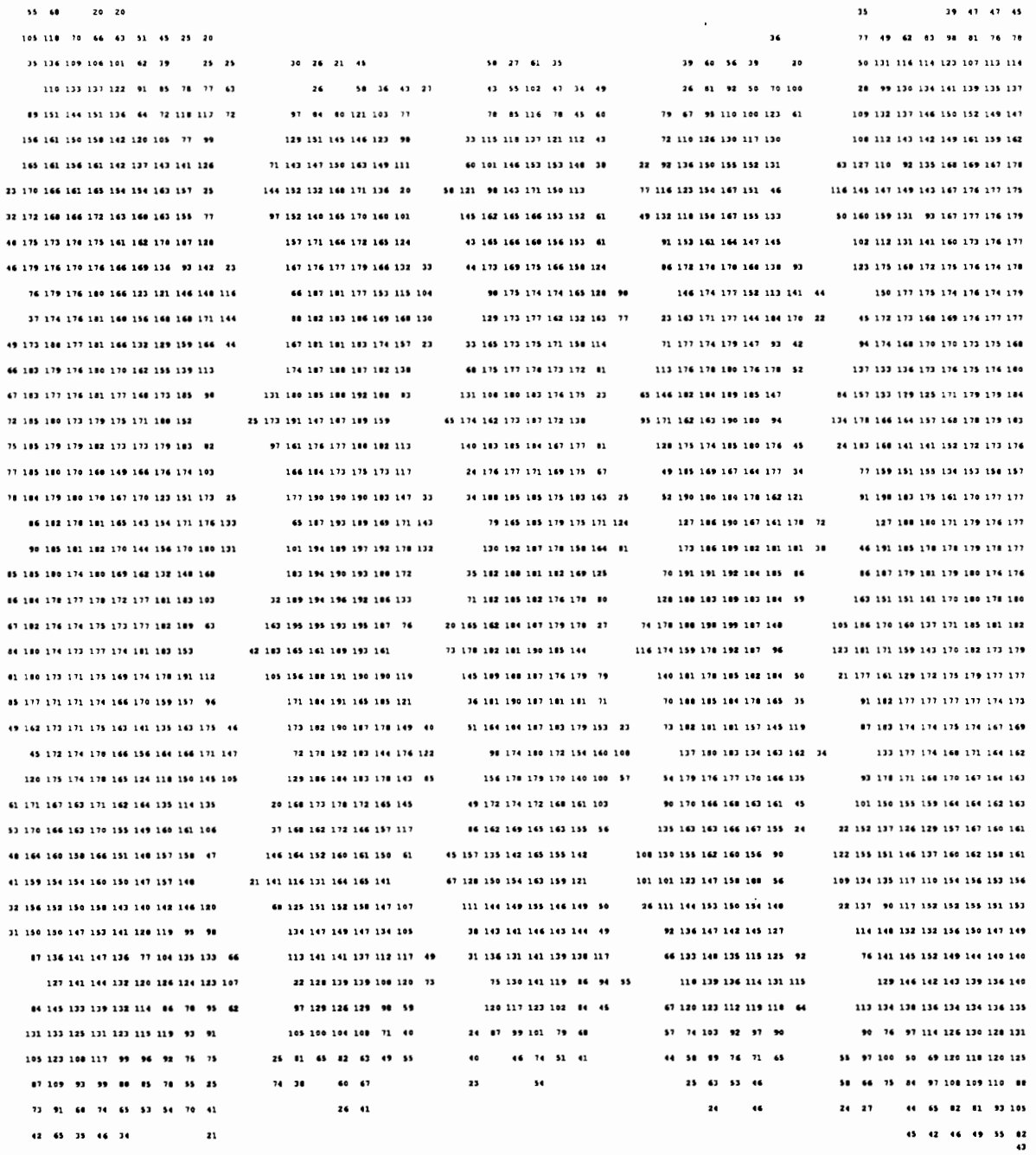

Fig 4.29. Numerical pressure map for the radial Michelin 255/70R/22.5 tire inflated to 110 psi and loaded to 8,000 pounds. The pressure print is 9.69 inches long and 7.91 inches wide

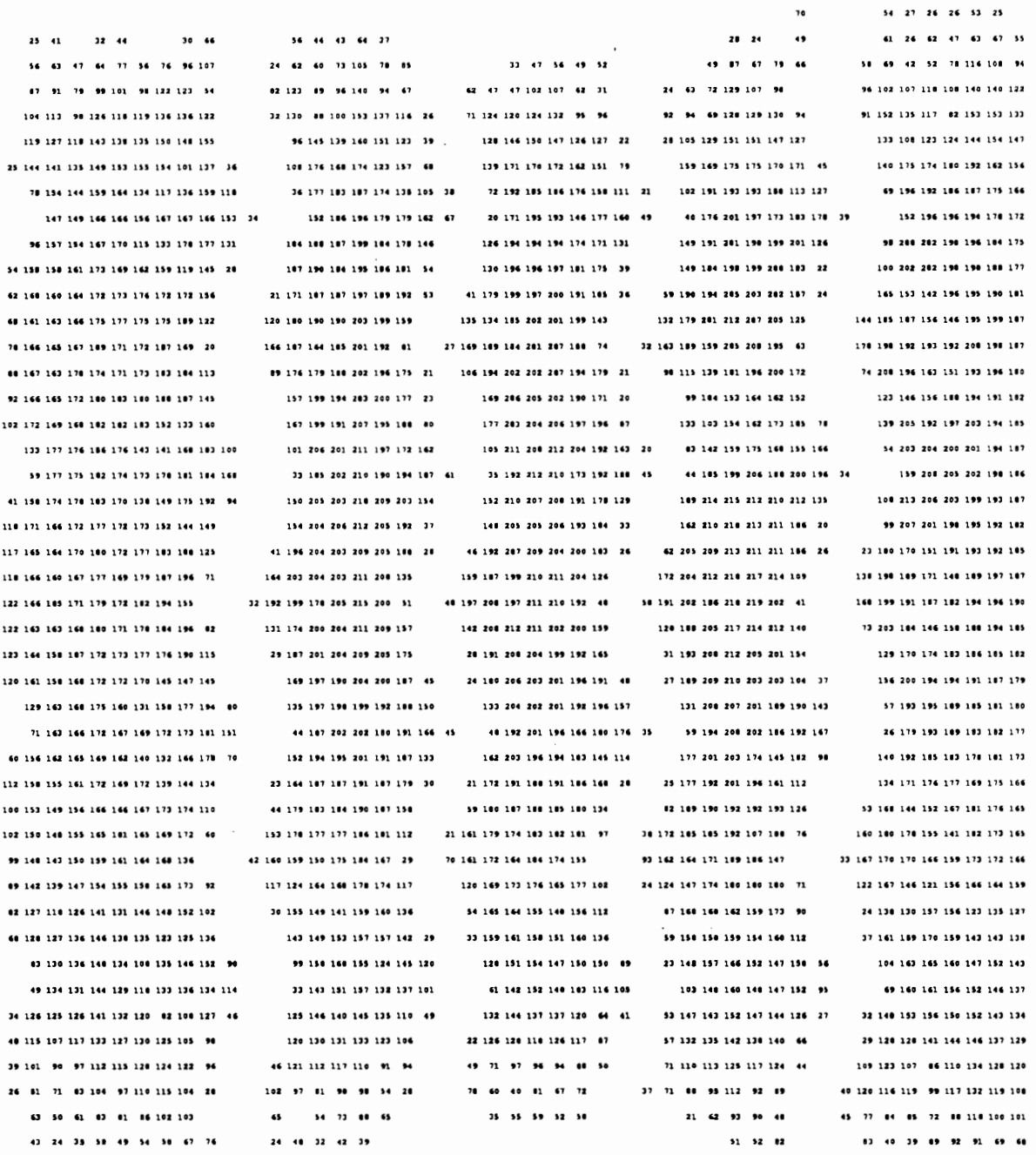

Fig 4.30. Numerical pressure map for the radial Michelin 255/70R/22.5 tire inflated to 135 psi and loaded to 8,000 pounds. The pressure print is 8.74 inches long and 7.91 inches wide.

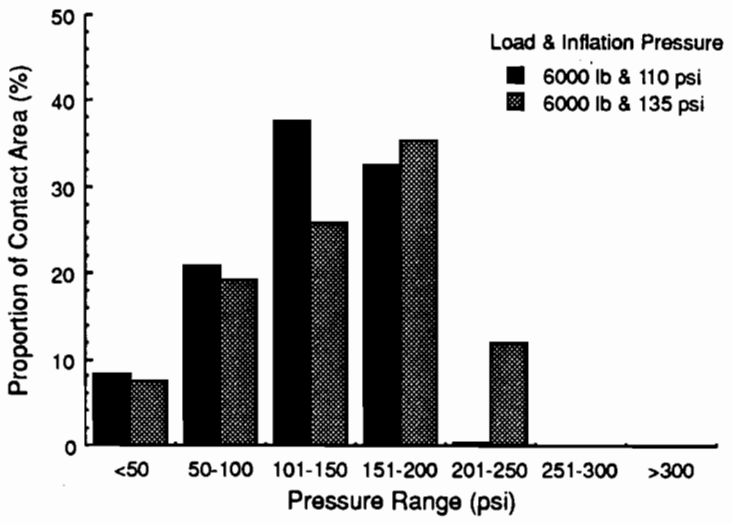

Fig 4.31. Histogram for the radial Michelin 255/70R/22.5 tire. Shown are the proportions of contact area at the various contact pressure ranges at a 6,000-pound wheel load and inflation pressures of 110 and 135 psi.

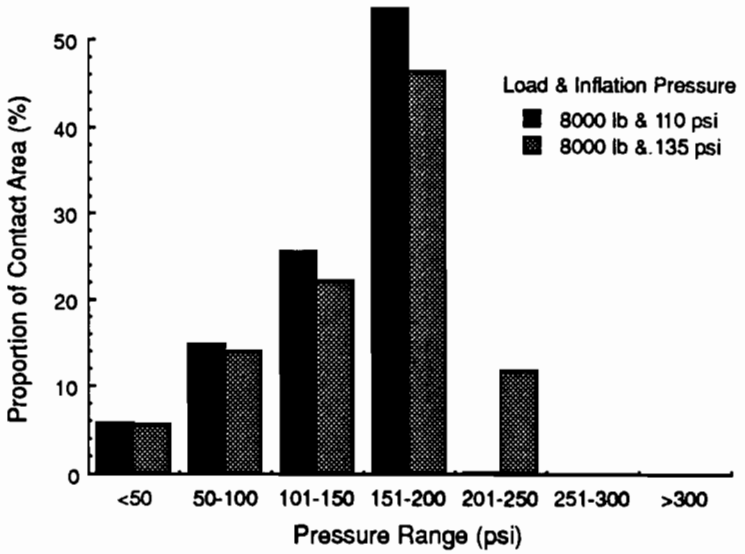

Fig 4.32. Histogram for the radial Michelin 255/70R/22.5 tire. Shown are the proportions of contact area at the various contact pressure ranges for a 8,000-pound wheel load and inflation pressures of 110 and 135 psi.

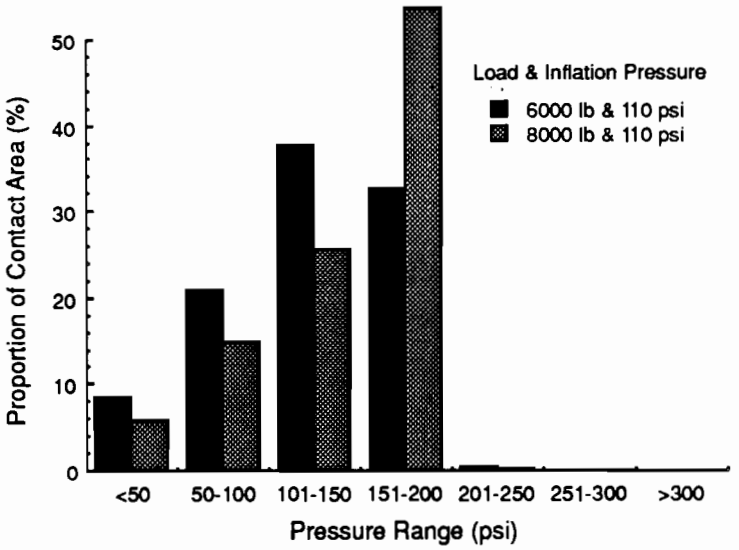

Fig 4.33. Histogram for the radial Michelin 255/70R/22.5 tire. Shown are the proportions of contact area at the various contact pressure ranges for an inflation pressure of 110 psi and wheel loads of 6,000 and 8,000 pounds.

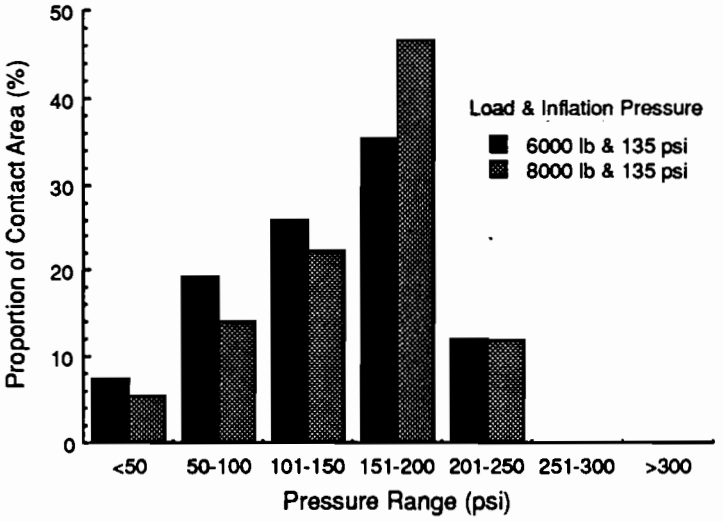

Fig 4.34. Histogram for the radial Michelin 255/70R/22.5 tire. Shown are the proportions of contact area at the various contact pressure ranges for an inflation pressure of 135 psi and wheel loads of 6,000 and 8,000 pounds.

TABLE 4.12. RADIAL GOODYEAR 11R24.5 PROPORTIONS OF CONTACT AREA (PERCENT) FOR THE 6,000 AND 8,000 LOADS

Pressure Ranges (psi)	6,000-lb Load		8,000-lb Load	
	Inflation Pressure			
	95 psi	110 psi	95 psi	110 psi
< 50	14.11	9.13	10.94	6.58
50-100	36.79	43.80	28.12	40.82
101-150	42.67	33.80	35.51	31.38
151-200	6.43	12.77	23.87	16.88
201-250	0.00	0.50	1.56	4.08
251-300	0.00	0.00	0.00	0.26
>300	0.00	0.00	0.00	0.00

TABLE 4.13. RADIAL GOODYEAR 11R24.5 LOAD DISTRIBUTION (LB) ACROSS THE TREADWIDTH FOR 6,000 AND 8,000 POUNDS

Position Tread Width	6,000-lb Load		8,000-lb Load	
	Inflation Pressure			
	95 psi	110 psi	95 psi	110 psi
Left	1115.3	1252.5	1662.8	1916.6
Left-Center	1130.5	1037.9	1408.2	1270.6
Center	1542.7	1498.4	1857.3	1746.2
Right-Center	1090.1	962.2	1350.6	1192.4
Right	1121.4	1249.0	1721.1	1874.2

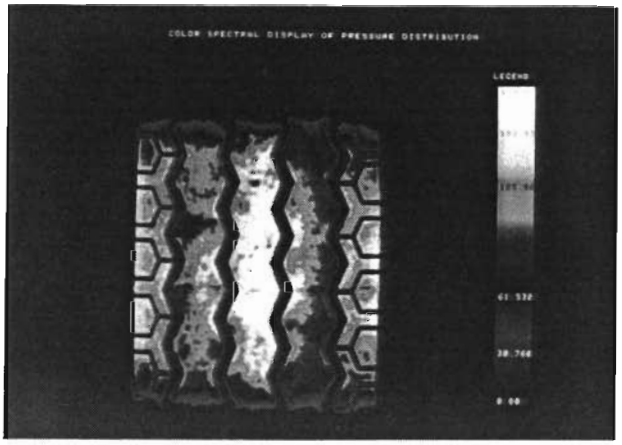

Fig 4.35. Two-dimensional contact pressure plot for the radial Goodyear 11R24.5 LR-G tire inflated to 95 psi and loaded to 6,000 pounds.

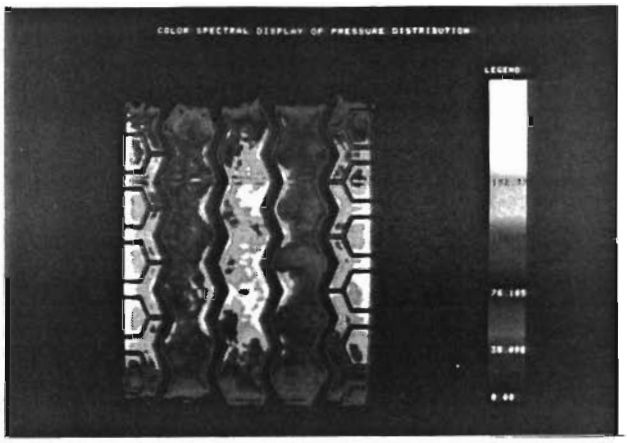

Fig 4.36. Two-dimensional contact pressure plot for the radial Goodyear 11R24.5 LR-G tire inflated to 110 psi and loaded to 6,000 pounds.

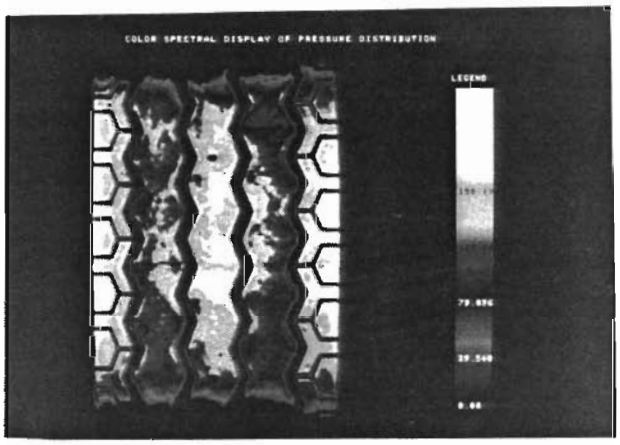

Fig 4.37. Two-dimensional contact pressure plot for the radial Goodyear 11R24.5 LR-G tire inflated to 95 psi and loaded to 8,000 pounds.

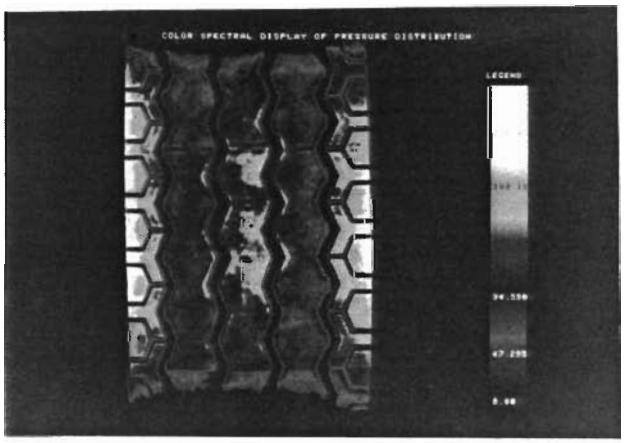

Fig 4.38. Two-dimensional contact pressure plot for the radial Goodyear 11R24.5 LR-G tire inflated to 110 psi and loaded to 8,000 pounds.

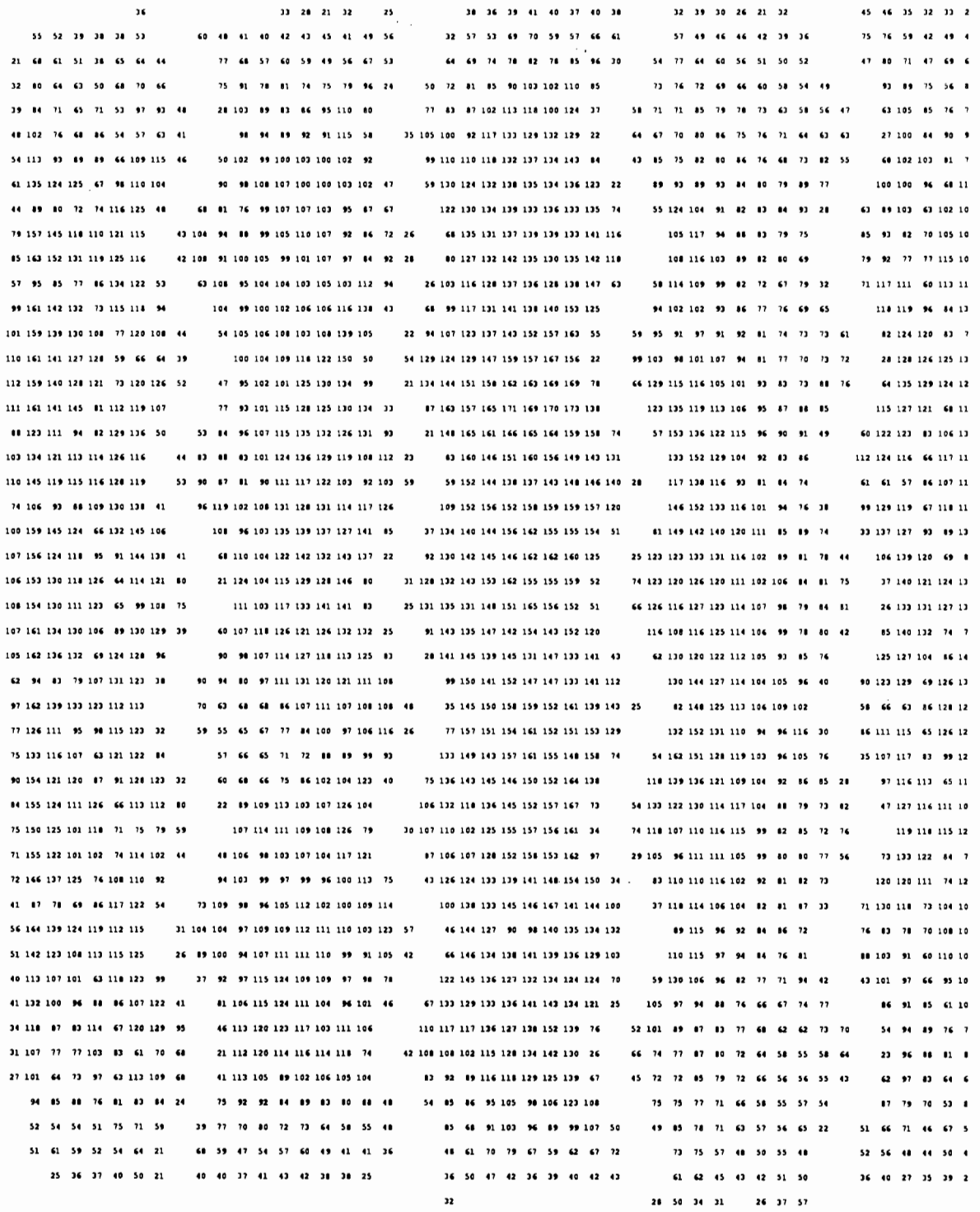

Fig 4.39. Numerical pressure map for the radial Goodyear 11R24.5 tire inflated to 95 psi and loaded to 6,000 pounds. The pressure print is 9.65 inches long and 7.48 inches wide.

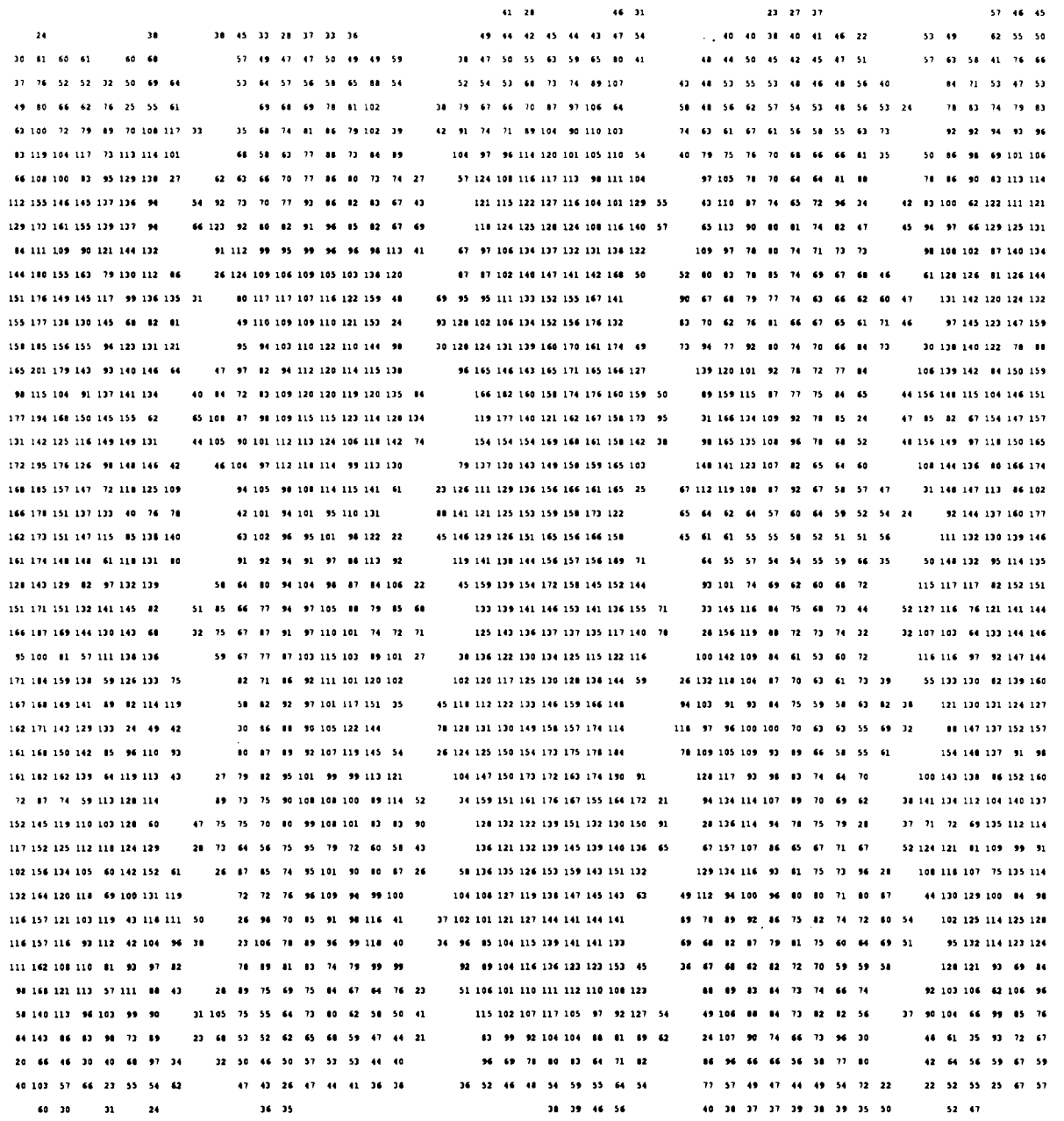

Fig 4.40. Numerical pressure map for the radial Goodyear 11R24.5 tire inflated to 110 psi and loaded to 6,000 pounds. The pressure print is 9.2 inches long and 7.48 inches wide.

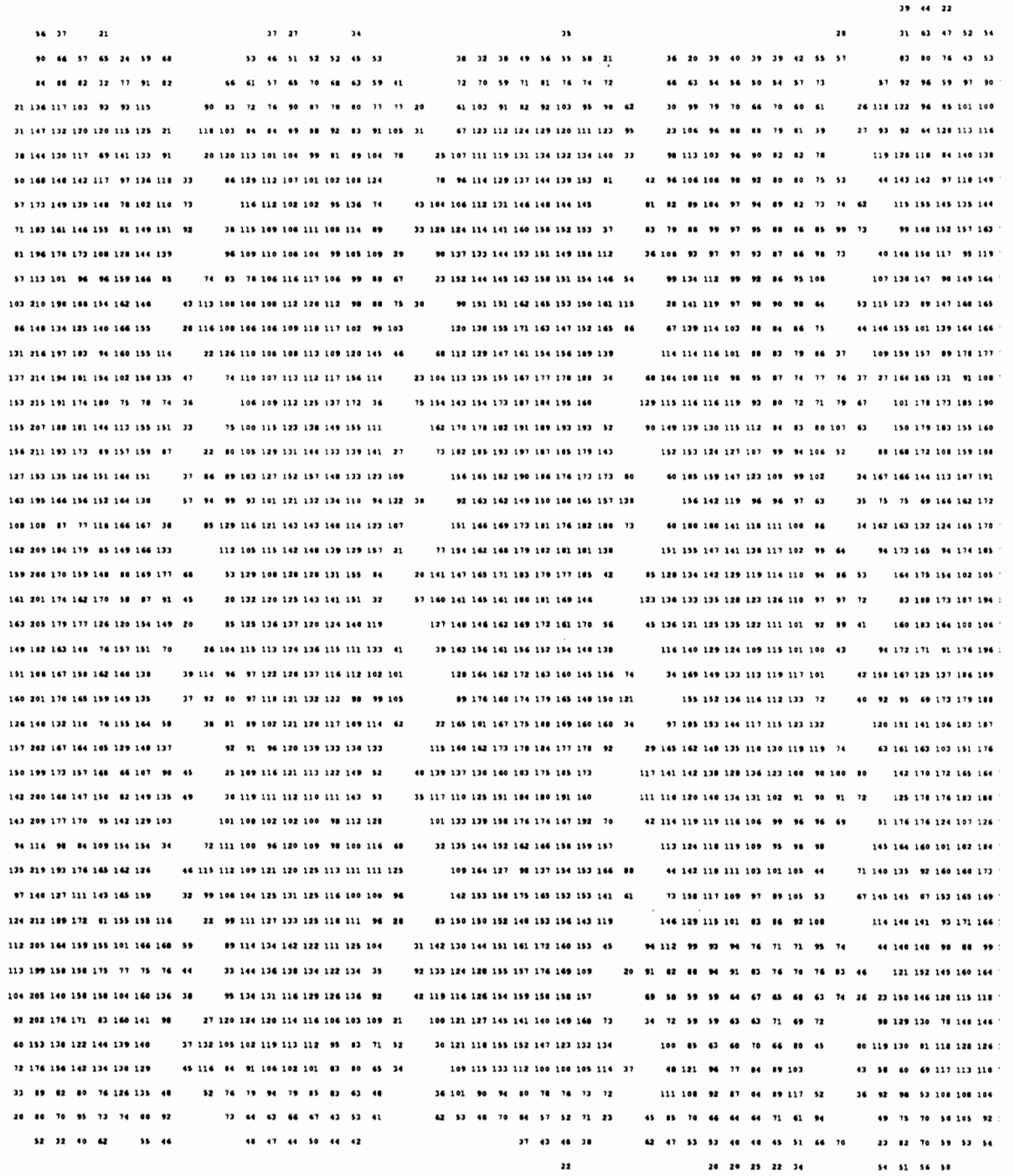

Fig 4.41. Numerical pressure map for the radial Goodyear 11R24.5 tire inflated to 95 psi and loaded to 8,000 pounds. The pressure print is 11.14 inches long and 7.48 inches wide.

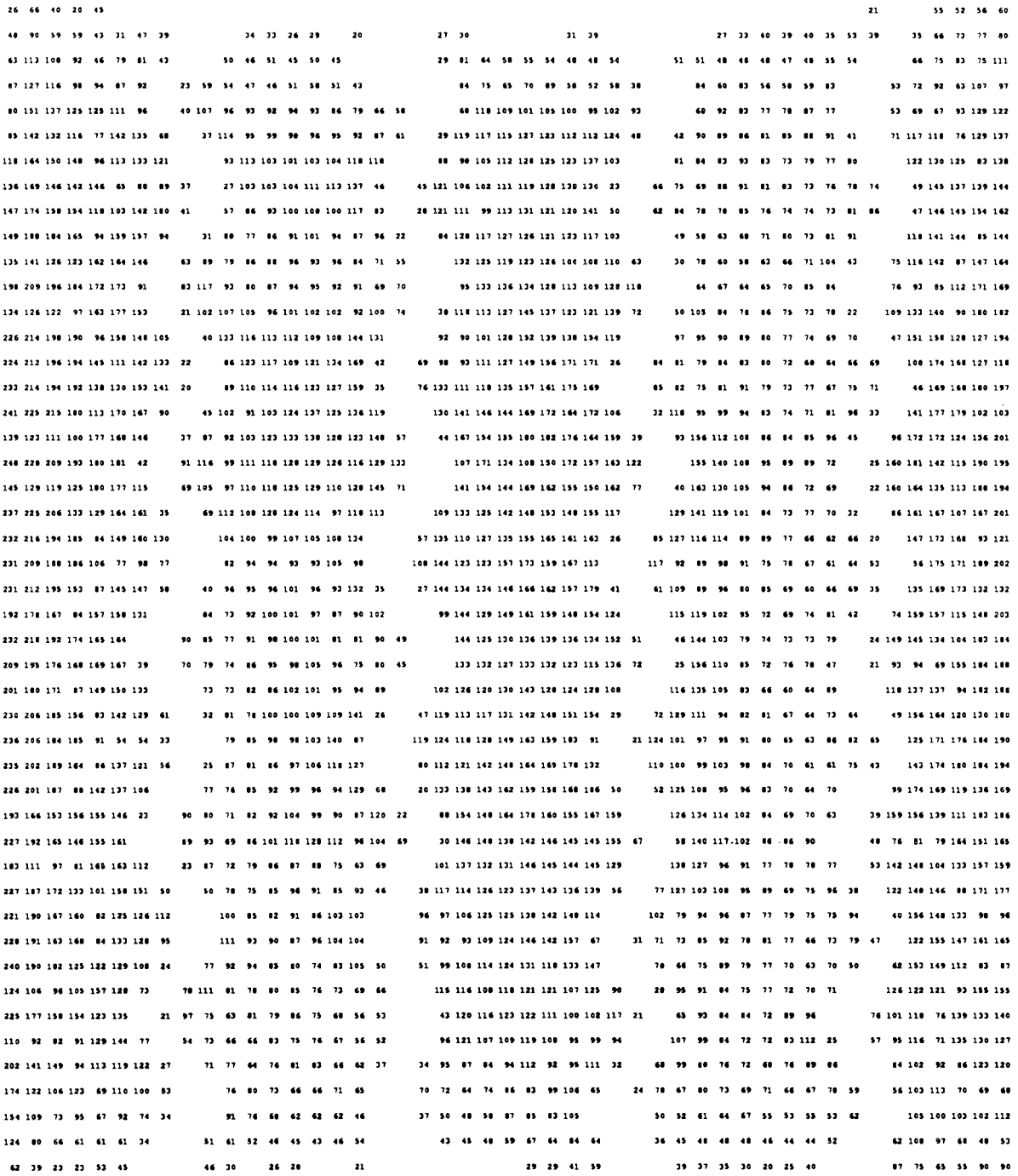

Fig 4.42. Numerical pressure map for the radial Goodyear 11R24.5 tire inflated to 110 psi and loaded to 8,000 pounds. The pressure print is 10.63 inches long and 7.48 inches wide.

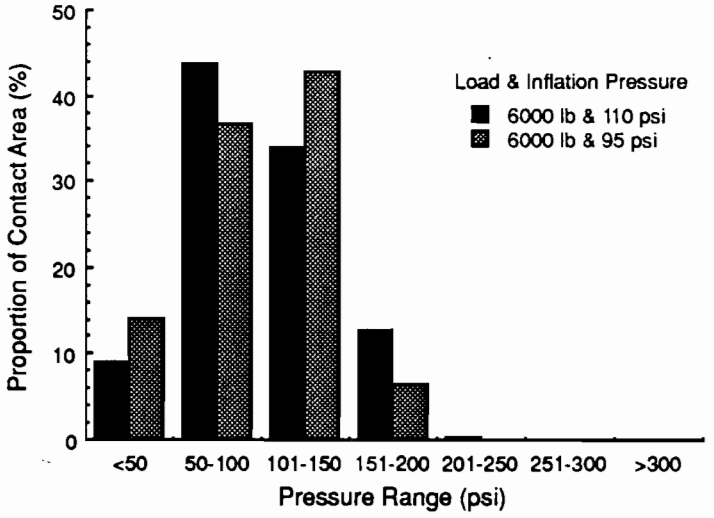

Fig 4.43. Histogram for the radial Goodyear 11R24.5 tire. Shown are the proportions of contact area at the various contact pressure ranges at a 6,000-pound wheel load and inflation pressures of 95 and 110 psi.

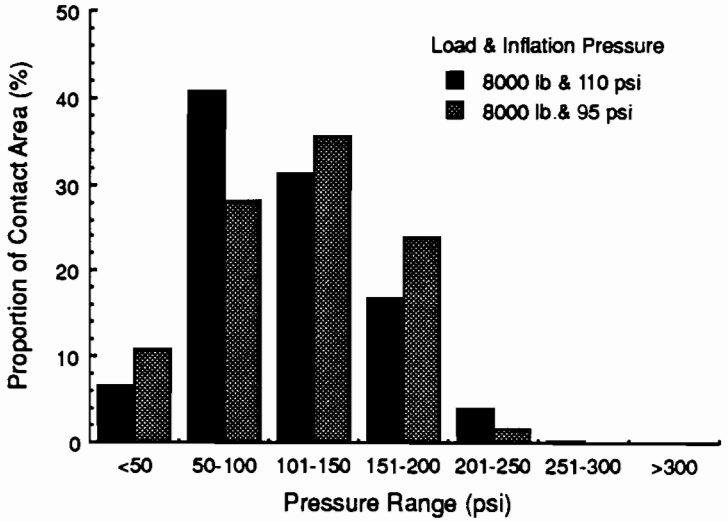

Fig 4.44. Histogram for the radial Goodyear 11R24.5 tire. Shown are the proportions of contact area at the various contact pressure ranges for a 8,000-pound wheel load and inflation pressures of 95 and 110 psi.

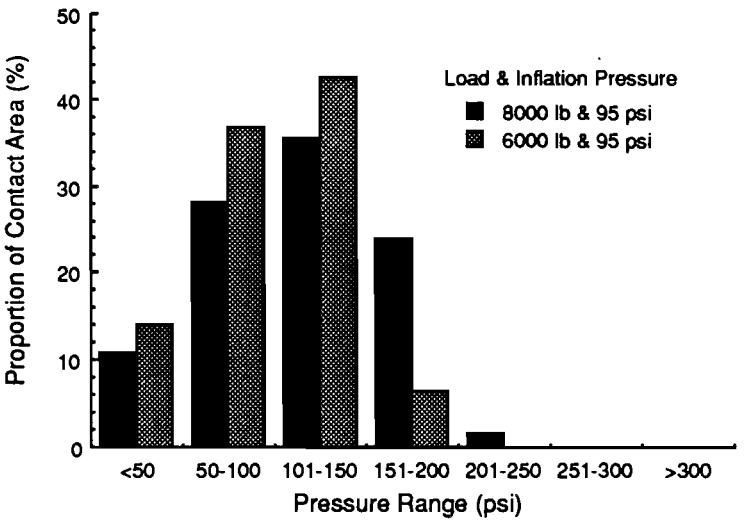

Fig 4.45. Histogram for the radial Goodyear 11R24.5 tire. Shown are the proportions of contact area at the various contact pressure ranges for an inflation pressure of 95 psi and wheel loads of 6,000 and 8,000 pounds.

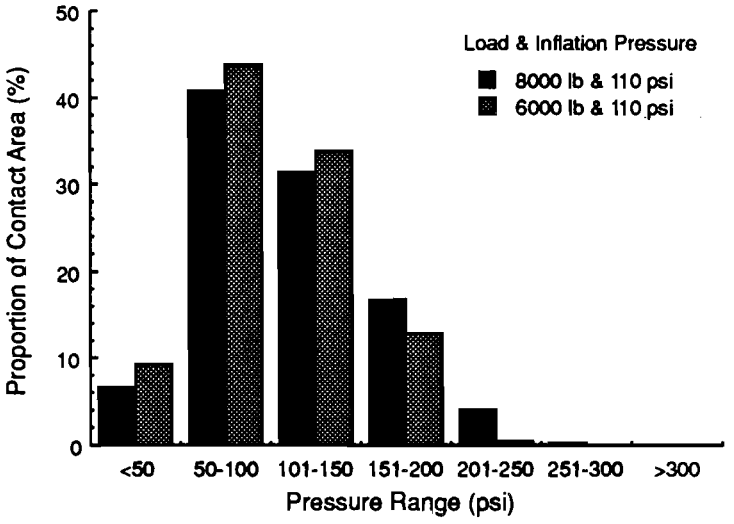

Fig 4.46. Histogram for the radial Goodyear 11R24.5 tire. Shown are the proportions of contact area at the various contact pressure ranges for an inflation pressure of 110 psi and wheel loads of 6,000 and 8,000 pounds.

CHAPTER 5. DISCUSSION AND ANALYSIS OF RESULTS

Based on the experimental results presented in Chapter 4, several observations can be made. The tire contact areas and contact pressure distributions are analyzed and discussed in this chapter. The measurements of the tire stiffness and side tire movements, presented in Appendix B, are also discussed.

TIRE CONTACT AREA

In pavement design procedures, the tire contact area is assumed to be the ratio of the wheel load over the tire inflation pressure. Tire contact area measurements from the testing were presented in Chapter 4, and those results are discussed and analyzed here.

Discussion of Results

The tire contact areas obtained from the Adage system and the counting method, the print width and print length of the contact areas, and the mean contact pressures are tabulated in Tables 4.1, 4.5, 4.8, and 4.11, for various combinations of inflation pressures and wheel loads. These experimental measurements of the tire contact areas reinforce Hansen's conclusion that, at a constant tire inflation pressure, an increase in wheel load is accompanied by an increase in the tire contact area, and, in the same way, that at a constant wheel load, an increase in tire inflation pressure is accompanied by a decrease in the tire contact area.

The same trend can be observed from the tire print dimensions. As the wheel load increases, the print width and the print length increase until the print width equals the tire width. Then, only the print length increases. In general, this behavior was expected due to the shape and the extraordinary elastic properties of tires.

The shape of the tire contact area was also observed. As stated by Hansen (Ref 1), the shape of the tire contact area for bias tires tends to become more oval, while for the radial tires the shape is consistently rectangular. This clear distinction in the shape of the tire contact areas must be noted, since pavements are designed assuming that this shape is circular. Modifications in these assumptions are imperative, since, as stated in Chapter 2, radial tires are becoming increasingly predominant in the market. In order to address this situation, the tire contact area values were subjected to further analysis.

Analysis of Results

A statistical model was constructed to relate the actual tire contact areas with the ratio of the wheel load over the tire inflation pressure. Here, this ratio is called the "Relative Area." To construct this statistical model it was decided to use the average of the tire contact areas obtained from the Adage system and the counting method. In this model, the tire contact area is the dependent variable and the relative area is the independent variable. The model is presented in Fig 5.1.

The proposed model is

$$TCA = 0.28905 + 1.0627\,(RA) - 0.00202\,(RA)^2$$

where

TCA = the tire contact area in square inches, and
RA = the relative area in square inches.

The statistical model was developed to predict the tire contact area in square inches, based on the ratio (also in square inches) of the wheel load over the tire inflation pressure. Even though the model did not consider factors such as tire wear, tire brand, and tire type, it has a very high correlation factor of 94 percent, using a 95 percent confidence interval. Figure 5.1 compares this model with the theoretical assumption that the relative area equals the tire contact area (the line having 45° slope).

Figure 5.1 brings to light several interesting facts. The theoretical assumption holds for relative areas below 50 square inches. As the wheel load increases, the accuracy of the theoretical assumption decreases. As the inflation pressure increases, the accuracy of the theoretical assumption increases.

This model can be used to arrive at a quick estimate of the actual contact area, based on easily obtainable parameters such as wheel load and tire inflation pressure. However, more testing and analysis needs to be done to obtain a more representative model, since this study was limited to only 20 observations.

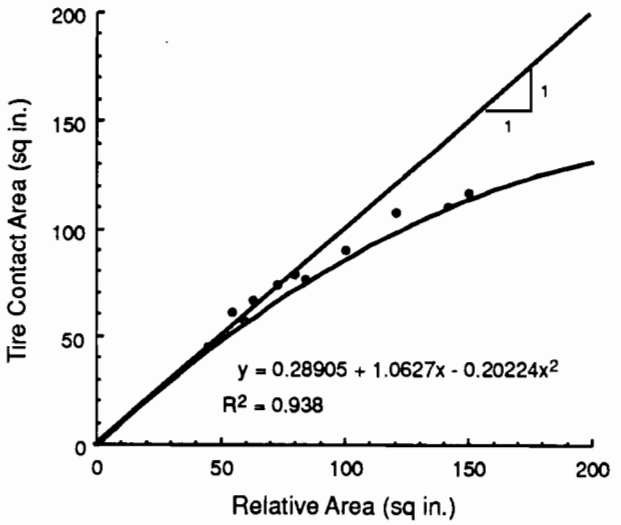

Fig 5.1. Tire contact area vs relative area. Shown is the predicting curve of the tire contact area based on the ratio of wheel load over inflation pressure (relative area).

TIRE CONTACT PRESSURE DISTRIBUTIONS

Tire contact pressure distributions are at present not being considered in pavement design procedures. It is assumed that any load transmitted from the tire to the pavement is uniformly distributed and equal to the tire inflation pressure. This obviously is a fallacy, since Tables 4.1, 4.5, 4.8, and 4.11 show that, in general, the mean contact pressures are higher than the actual tire inflation pressures. Experimentally it has been proved that high contact pressures are produced at the tire-pavement interface.

Figures 4.1, 4.2, 4.11, 4.12, 4.13, 4.14, 4.23, 4.24, 4.25, 4.26, 4.35, 4.36, 4.37, and 4.38 present two-dimensional color pressure plots for the different tires tested in this report. These color pressure plots represent the contact pressure distributions produced at the tire-pavement interface. The same information is presented in Figs 4.3, 4.4, 4.15, 4.16, 4.17, 4.18, 4.27, 4.28, 4.29, and 4.30 as numerical pressure maps.

For the tires tested, it can be seen that the higher contact pressure values are located generally at the edges of the treads located at the center and edges of the middle portion of the tire print.

For the bias Goodyear 18-22.5 tire, Figs 4.1 and 4.2 show the tire contact pressure distributions when the tire is loaded to 15,000 pounds and inflated to 100 and 85 psi respectively. The proportion of the contact area at higher pressure ranges increases with inflation pressure. Figures 4.1 and 4.2 do not record the peak contact pressure values, since they exceeded the capacity of the Fuji Super Low film range with which they were obtained. The proportions of contact area at each pressure range are obtained from the Fuji Super Low, and the Fuji Low film and are tabulated in Table 4.2.

For the radial Michelin 275/80R/24.5 tire, Figs 4.11, 4.12, 4.13, and 4.14 show the variations in the tire contact pressure distributions when the tire is subjected to different wheel loads and inflation pressures. Surprisingly, the peak pressure values were found at lower tire inflation pressures; however, the difference in the peak pressure values is very small.

For the radial Michelin 255/70R/22.5 tire, Figs 4.23, 4.24, 4.25, and 4.26 show the variations in the tire contact pressure distributions. As expected, the peak pressure values were found at higher tire inflation pressures.

For the radial Goodyear 11R24.5 tire, Figs 4.35, 4.36, 4.37, and 4.38 show the variations in the tire contact pressure distributions. As expected, the peak pressure values were found at higher tire inflation pressures.

In order to discuss and analyze the effect of the tire contact pressure distributions, the proportions of contact area at different pressure ranges were calculated. The load distribution along the tread width was also computed.

PROPORTIONS OF CONTACT AREA

Discussion

Tables 4.2, 4.3, 4.6, 4.9, and 4.12 show the proportions of contact area covered by the various pressure ranges for the different experimental parameters selected in this report. Data from these tables were used to construction the histograms in Figs 4.5 through 4.10 for the bias Goodyear 18-22.5 tire, Figs 4.19 through 4.22 for the radial Michelin 275/80R/24.5 tire, Figs 4.31 through 4.34 for the radial Michelin 255/70R/22.5 tire, and Figs 4.43 through 4.46 for the radial Goodyear 11R24.5 tire. In general, a trend was observed. For a given wheel load, as the inflation pressure decreases, the proportions of contact area at lower contact pressure ranges increase, and, as the inflation pressure increases, the proportions of contact area at higher contact pressure ranges increase. Similarly, for a given inflation pressure, as the wheel load decreases, the proportion of contact area at lower contact pressure ranges increases, and, as the wheel load increases, the proportion of contact area at higher contact pressure ranges increases.

Due to changes in the wheel load and in the tire inflation pressure, tire contact pressures will be distributed differently over the contact area. Tire contact pressure distributions, evaluated for various contact pressure ranges, show several cases in which the critical ones will be those where higher proportions of contact area are at higher contact pressure ranges.

Analysis

Based on this trend a model for estimating an equivalent contact pressure number capable of measuring the effects of changes in tire inflation pressures and static wheel loads was developed. This number estimates equivalencies of contact pressures for different sets of wheel loads and tire inflation pressures. For example, a tire with a wheel load (A) and an inflation pressure (B) can produce the same effect as the tire with a wheel load (C) inflated to (D). With this purpose, an equivalent contact pressure model was developed using principles of fatigue theory.

Lay (Ref 31) suggests the use of the fourth power law in comparing different types and tire configurations for pavement damage. In general, the fourth power law is invoked when a new configuration produces a different criterion strain or deflection to the standard one. The AASHO road test (Refs 12 and 32) used the fourth power law in developing the equivalency factors. However, the AASHO road test did not consider the actual tire-pavement contact pressure distributions to estimate pavement damage, because AASHO developed those factors in terms of axle loads only. Therefore, to estimate better pavement damage, the fourth power law will be used in order to take into account actual tire-pavement contact pressure distributions.

The proposed model is termed equivalent contact pressure number (ECPN) and varies proportionally with the summation of the contact pressure ranges to the fourth power, times the contact areas of each contact pressure range and divided by a standard reference. A wheel loadof 10,000 pounds distributed uniformly over an area of 100 square inches was the chosen reference, because 10,000-pound wheel load appears to be the trend in wheel load regulations for various states (Ref 16). The ECPN model uses the proportions of contact area values because the total tire contact area has been factored and located out of the summation.

$$ECPN = \frac{\sum_{i=1}^{n} f_i \times \overline{PR_i}^4}{P_r^4} \times \frac{TCA}{Ar}$$

where

E_w = the weighted number computed at each set of wheel load and tire inflation pressure,

f_i = the proportion of contact area at the pressure range i,

$\overline{PR_i}$ = the mean of the contact pressure range,

P_r = the chosen reference contact pressure (P_r = 100 psi was used),

TCA = the tire contact area, and

A_r = the chosen reference contact area (A_r = 100 square inches was used).

Using this method, the ECPN number was calculated at each experimental parameter for all the tires tested. Table 5.1 shows the calculated ECPN values.

ECPN values are characterized for a particular set of parameters which limit our experimental results. Several regression models were also developed to predict proportions of contact area for each pressure range based only on the wheel loads and tire inflation pressures, and neglecting sizes, brands, and types of tires. However, those models were found unsatisfactory due to the limited number of observations. But, with further testing and analysis, this procedure could be applied with greater success, as graphically described in Figs 5.2 and 5.3.

Figures 5.2 and 5.3 show the correlation between the ECPN and the tire inflation pressure at different wheel loads for the radial Goodyear 11R24.5 tire and the radial Michelin 255/70R/22.5 tire, respectively. Assuming that the behavior of the ECPN is linear for a constant wheel load, the radial Goodyear 11R24.5 tire will have the same equivalent contact pressure number when inflated to 50 psi and having an 8,000-pound load, as when it is inflated to 150 psi and having a 6,000-pound load; and, because they have the same ECPN, it can be estimated that those cases will produce similar pavement damage and that resulting damage will double the damage caused by a wheel load of 10,000 pounds uniformly distributed over an area of 100 square inches. Similarly, it can be estimated that the radial Michelin 255/70R/22/5 tire will produce the same pavement damage when inflated to 100 psi and having an 8,000-pound load, as when it is inflated to 130 psi and having a 6,000-pound load. The pavement damage will be equal to three times the damage caused by a wheel load of 10,000 pounds uniformly distributed over an area of 100 square inches.

TABLE 5.1. ECPN NUMBER FOR THE TIRE EXPERIMENTAL PARAMETERS

Tire Type	Inflation Pressure (psi)	Loads (lb)	ECPN
18 - 22.5B	85	8,000	3.001
	85	10,000	3.637
	85	12,000	3.907
	85	15,000	9.269
	100	8,000	3.699
	100	10,000	4.852
	100	12,000	3.819
	100	15,000	10.093
275/80R/24.5	95	6,000	2.284
	95	8,000	4.506
	110	6,000	2.097
	110	8,000	4.144
255/70R/22.5	110	6,000	2.073
	110	8,000	3.488
	135	6,000	3.204
	135	8,000	4.831
11R24.5	95	6,000	1.170
	95	8,000	2.542
	110	6,000	1.398
	110	8,000	2.707

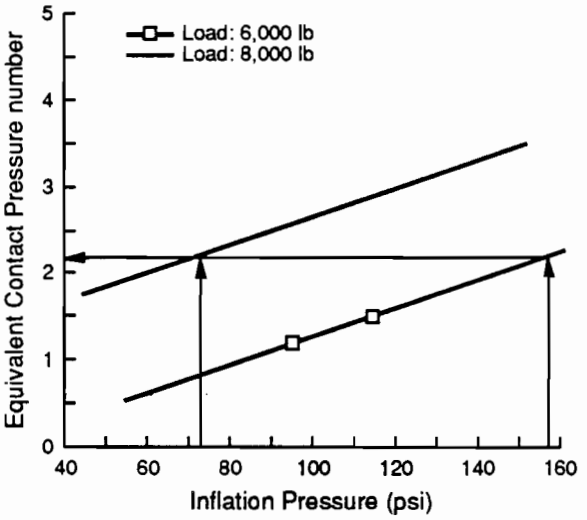

Fig 5.2. Graph of the equivalent contact pressure number (ECPN) vs tire inflation pressure at different wheel loads, for the radial Goodyear 11R24.5 tire.

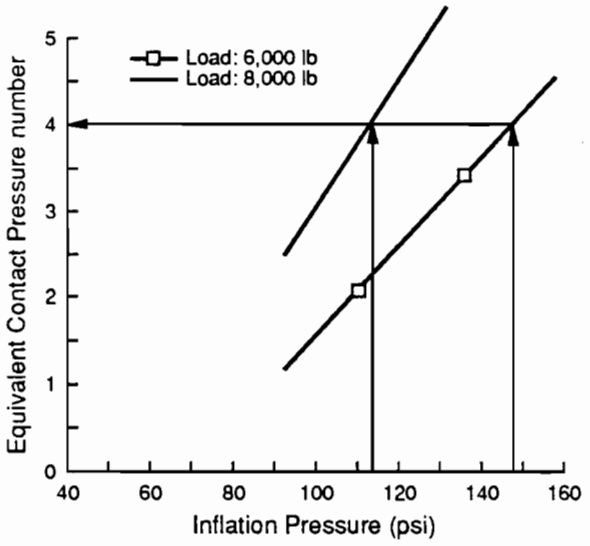

Fig 5.3. Graph of the equivalent contact pressure number (ECPN) vs tire inflation pressure at different wheel loads, for the radial Michelin 255/70R/22.5 tire.

This model which qualitatively measures pavement damage in terms of an equivalent contact pressure number (ECPN), holds promise if further testing and analysis are available to support the method.

Comparison Between the Tires

The proportions of contact area at the various pressure ranges are compared for the different tires at approximately the same set of experimental parameters. Figure 5.4 shows the comparison.

Figure 5.4 shows that, for roughly the same parameters, the radial Michelin 255/70R/24.5 tire has a higher proportion of the contact area at the 151-200 psi pressure range than the other tires. In general, the bias Goodyear 18-22.5 tire, the radial Michelin 275/80R/24.5 tire, and the radial Goodyear 11R24.5 tire have approximately the same proportions of contact area at the various contact pressure ranges. This similarity must be investigated further.

Obviously, to determine what tire is causing the most damage to the pavements requires that a fatigue concept be introduced for analyzing the proportion of the contact areas at each pressure range. This concept needs to be refined in order to estimate the effects of tire types and/or brands.

LOAD DISTRIBUTION ALONG THE TREAD WIDTH

Another aspect of interest was the load distribution along the tread width. In general, as stated before, the largest portion of the total wheel load is generally located at the center tread region. Tables 4.4, 4.7, 4.10, and 4.13 record the values for the different distribution of the load along the tread width of tires as obtained through the Adage system. No patterns or trends can be observed.

TIRE VERTICAL STIFFNESS

The tire vertical stiffness is defined as the ratio of the wheel load over the total vertical deformation of the tire. Tables B.1 through B.8 (in Appendix B) record the measurements of the tire vertical stiffness, as well as the sidewall movements. These measurements will serve other researchers in the comparison and calibration of their analytical estimations of tire vertical stiffness and tire deformations.

Discussion

In general, it was found that the tire vertical stiffness is directly influenced by the tire inflation pressure. As the inflation pressure increases, the tire vertical stiffness increases, and the side tire movement decreases. In order to estimate the tire vertical stiffness in terms of the wheel load and tire inflation pressure, a statistical analysis was performed.

Analysis of Results

Several regression models were developed in order to estimate the tire vertical stiffness in terms of the relative

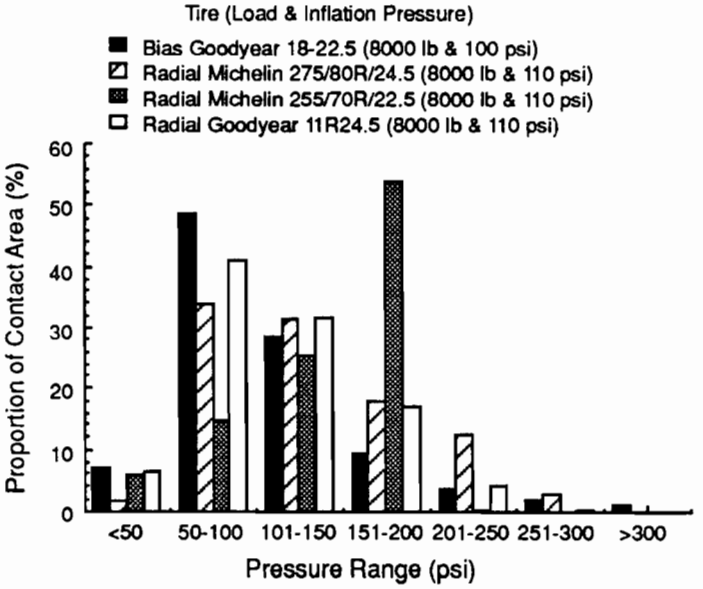

Fig 5.4. Histogram for all the tires. Shown is a comparison of the proportions of contact area at various contact pressure ranges for the tires tested.

area, tire contact area, and wheel load. The best model used the tire contact area as the independent variable and had a correlation coefficient of 63.3 percent. As discussed in Chapter 2, the tire vertical stiffness depends on many factors, such as tire construction, tire wear, tire type, wheel load, and tire inflation pressure; hence, correlation values were not expected to be very high. This model is recommended in case no better information is available. The model clearly needs to be improved, either by testing more tires or by considering more predictor variables, in order to establish multi-regression models. The proposed model is

$$TVs = 3.252 + 0.031 \times TCA - 0.000058 \times TCA^2$$

where

TVs = the tire vertical stiffness in kips/inch, and
TCA = the tire contact area in square inches.

Figure 5.5 shows the relationship between the tire vertical stiffness and the tire contact area. The designer should first calculate the relative area and then use Fig 5.1 to determine the tire contact area, in order to estimate the tire vertical stiffness from Fig 5.5.

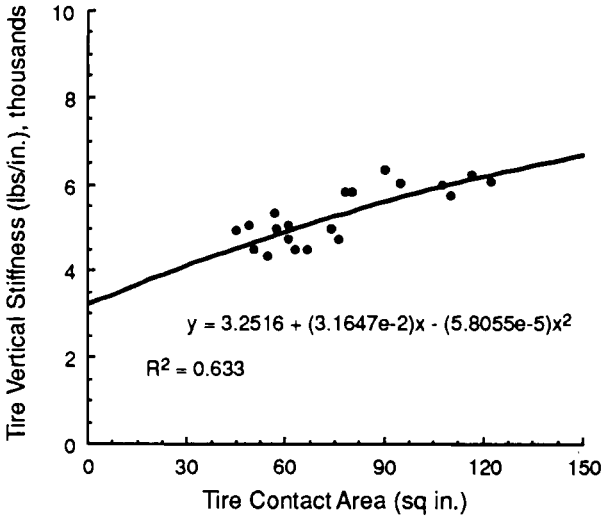

Fig 5.5. Graph of the tire vertical stiffness vs. the tire contact area showing the predicting curve of the tire vertical stiffness based on the tire contact area of the tire.

CHAPTER 6. CONCLUSIONS AND RECOMMENDATIONS

CONCLUSIONS

(1) For bias tires, the shape of the contact area is more circular than that for radial tires, and it becomes more oval as the wheel load increases. In contrast, for radial tires, the shape of the contact area is consistently rectangular.

(2) The tire contact area, irrespective of tire construction and tire type, can be determined from a parameter called the relative area, which is the ratio of the wheel load over the tire inflation pressure.

(3) For a given wheel load, as the inflation pressure decreases, the proportions of contact area at lower contact pressure ranges increase; and, as the inflation pressure increases, the proportions of contact area at higher contact pressure ranges increase. Similarly, for a given inflation pressure, as the wheel load decreases, the proportions of contact area at lower contact pressure ranges increases; and, as the wheel load increases, the proportions of contact area at higher contact pressure ranges increases.

(4) As the wheel load increases, the print width and the print length increase until the print width equals the tire width. After that, only the print length increases.

(5) The higher contact pressure values are generally produced at the edge of the tread ribs, means are located at the center and edges of the middle portion of the tire print.

(6) In general, the mean contact pressures are higher than the tire inflation pressures.

RECOMMENDATIONS

The following recommendations for future research result from an evaluation of the study and the data:

(1) This study presents information on several aspects of tire-pavement contact pressure distributions. Several statistical models were developed during the course of this study. It is recommended that further testing be conducted to obtain a more representative sample in order to estimate tire contact pressure distributions for different wheel loads and tire inflation pressures.

(2) The data obtained from the numerical pressure maps should be used as the input for modeling pavement behavior. For instance, finite element models based on these data can be used to estimate statically induced stresses and strains in the pavement structure.

(3) Since very few experimental studies have been carried out with dynamic models of tire-pavement contact pressure distributions, these need to be investigated in future studies.

REFERENCES

1. Hansen, Rex, "Truck Tire Pavement Contact Pressure Distribution Characteristics for the 'Super Single' Bias 18-22.5 and 'Smooth' Radial 11R24.5 Tires," M. S. Thesis, The University of Texas at Austin, May 1989.
2. Chan, Gerard, "Computer Image Processing Technique for Analysis of the Tire Contact Pressures," M. S. Thesis, The University of Texas at Austin, December 1988.
3. Roberts, F. L., et al, "Establishing Material Properties for Thin Asphalt Concrete Surfaces on Granular Bases," Research Report 345-1, Texas Transportation Institute, Texas A&M University, College Station, Texas, November 1985.
4. van Vuuren, D. J., "Tire Pressure and Its Effect on Pavement Design and Performance," Civil Engineering In South Africa, Vol 16, No. 8, August 1974.
5. Brown, J. L., "Proceedings of a Symposium/Workshop on High Pressure Truck Tires," Austin, Texas, February 1987.
6. Butler, Lee, "Truck Tire Pressure and Pavement Damage," *Proceedings*, Symposium/Workshop on High Pressure Truck Tires, Austin, Texas, February 1987.
7. Wakeland, Richard E., "Video Image Analysis of Pressure Sensitive Film," M. S. Thesis, The University of Texas at Austin, December 1985.
8. Roberts, F. L., et al, "The Effect of Tire Pressures on Flexible Pavements," Research Report 372-1F, Texas Transportation Institute, Texas A&M University, College Station, Texas, August 1986.
9. Planning and Statistics Bureau, Montana Department of Highways, "1984 Truck Tire Study," Helena, Montana, 1984.
10. "Tire Pressure Survey," Unpublished Data, Bureau of Design, Division of Highways, Illinois Department of Transportation, Springfield, Illinois, 1986.
11. Thompson, Marshall R., "Analytical Methods for Considering Tire Pressure Effects in Pavement Design," *Proceedings*, Symposium/Workshop on High Pressure Truck Tires, Austin, Texas, February 1987.
12. AASHO Road Test, Highway Research Board, "History and Description of the Project," Report 61A, 1960.
13. Sharp, Asa, "Truck Tire Pavement Interaction," *Proceedings*, Symposium/Workshop on High Pressure Truck Tires, Austin, Texas, February 1987.
14. Clark, Samuel K., Editor, *Mechanics Of Pneumatic Tires*, National Bureau of Standards Monograph 122, November 1971.
15. Tielking, J. T., and F. L. Roberts, "Tire Contact Pressure and Its Effects on Pavement Strain," Journal of Transportation Engineering, Vol 113, No. 1, January 1987.
16. Sharma, J., and J. Mahoney, "Evaluation of Present Legislation and Regulations on Tire Sizes, Configurations and Load Limits," unpublished Executive Summary prepared by the University of Washington for the Washington Department of Transportation.
17. Lippmann, S. A., and K. L. Oblizajek, "The Distributions of Stress Between the Tread and the Road for Freely Rolling Tires," SAE 74102, Society of Automotive Engineers, Detroit, February 1974.
18. Papagianakis, A. T., and R. C. G. Haas, "Wide-Base Truck Tires: Industry Trends and State of Knowledge of Their Impact on Pavements," Ministry of Transportation and Communications of Ontario, December 1986.
19. Yeager, R. W., "Tires of the Nineties and Beyond," Elastomerics, Vol 119, No. 2, February 1987.
20. Seitz, N., and A. W. Hussmann, "Forces and Displacement in Contact Area of Free Rolling Tires," SAE Transaction, Vol 80, Paper No. 710626, 1971.
21. Bonse, R. P. H., and S. H. Kuhn, "Dynamic Forces Exerted by Moving Vehicles on a Road Surface," Highway Research Board Bulletin, No. 233, 1959.
22. Ginn, J. L., and R. L. Marlowe, "Road Contact Forces of Truck Tires as Measured in the Laboratory," SAE Transactions, Vol 76, Paper No. 670493, 1967.
23. Zekoski, J., "Impact of Truck Tire Selection on Contact Pressers," FHWA Load Equivalence Workshop, sponsored by the Federal Highway Administration Pavements Division, Turner-Fairbanks Highway Research Center, McLean, Virginia, September 13-15, 1988.
24. Huhtala, M., "Field Tests to Compare Tires," FHWA Load Equivalence Workshop, sponsored by the Federal Highway Administration Pavements Division, Turner-Fairbanks Highway Research Center, McLean, Virginia, September 13-15, 1988.

25. Marshek, K. M., et al., "Experimental Investigation of Truck Tire Inflation Pressure On Pavement-Tire Contact Area and Pressure Distribution," Research Report 386-1, Center For Transportation Research, The University of Texas at Austin, August 1985.

26. Haas, R. C. G., and A. T. Papagianakis, "Understanding Pavement Rutting," Roads and Transportation Association of Canada, Toronto, Ontario, September 28, 1986.

27. Eisenmann, J., and A. Hilmer, "Influence of Wheel Load and Inflation Pressure on the Rutting Effects at Asphalt-Pavements-Experiments and Theoretical Investigations," Sixth International Conference on the Structural Design of Asphalt Pavements, Ann Arbor, July 1987.

28. Monismith, C. L., "Fatigue Characteristics of Asphalt Paving Mixtures and Their Use in Asphalt Pavements," *Proceedings*, Annual Pavement Conference, Symposium on Fatigue In Asphalt Pavements, University of New Mexico, Albuquerque, New Mexico, 1981.

29. Chen, H. H., K. M. Marshek, and C. L. Saraf, "Effects of Truck Tire Contact Pressure Distribution on the Design of Flexible Pavements: A Three-Dimensional Finite Element Approach," Transportation Research Report 1095, Transportation Research Board, National Research Council, Washington, D. C., 1986.

30. "Fuji Prescale Film General Information," Fuji Photo Film Company, Limited, Tokyo, Japan, 1986.

31.. Lay, M. G., "Handbook of Road Technology," Vols 1 and 2, Gordon and Breach Science Publishers, Amsterdam, 1986.

32. Yoder and Witczak, "Principles of Pavement Design," Second Edition, John Wiley & Sons, New York, 1975.

APPENDIX A. EXPERIMENTAL AND ANALYTICAL PROCEDURES FOR DETERMINING TIRE CONTACT PRESSURE DISTRIBUTIONS

The tire contact pressure distributions were determined using certain experimental and analytical procedures, details of which are given below.

EXPERIMENTS

Experimental Equipment

The equipment used was the same as that used by Hansen. Complete details of the load frame, including the list of the parts for assembling purposes, can be found in Ref 1.

Load Cell Calibration

To determine the applied load, a Lebow 20-kip load cell was used. This load cell was calibrated against a Conamp 20 Digital Calibration system. This Conamp system displays a direct digital readout of the loads on the calibration cell. A calibration curve is needed to relate the voltages with the wheel loads. The calibration curve used by Hansen was used since the same load cell was used without any time gap. Details of the load cell calibration curve and the calibration procedure followed can be found in Ref 1.

Pressure Print Production

The procedure followed in producing the pressure prints of the tires tested under different loads and tire inflation pressures was the same as that detailed by Hansen (Ref 1). However, as explained in Chapter 3, the bias Goodyear 18-22.5 Super Single tire was tested using the Fuji Low range film, in addition to the Fuji Super Low range film, in order to record the higher contact pressure values which presumably were not recorded by the Fuji Super Low range film. This special strategy was employed only for the bias Goodyear 18-22.5, and not for other tires, since only a very small portion of the contact area was covered by pressures above 300 psi for this tire.

For the testing of the bias Goodyear 18-22.5, the Fuji Super Low range film was placed at the bottom of the two. Both sets of films recorded pressure distributions under the same conditions but required different calibration curves, due to the difference in the pressure range capacity of each film. Hence, the analysis of each film was performed independently.

ANALYSIS

Adage System Analysis

The tire prints were digitized using a scanner and were displayed on the Adage system monitor. Several computer programs were written on the Adage system exclusively for analyzing the tire prints. The procedure for analyzing the tire prints using the Adage system consists of five steps: (1) set up the scanner, (2) execute the programs, (3) create a filter, (4) construct a calibration curve, and (5) perform the tire print analysis.

In general, at each session the lighting and scanner settings were not altered once the filter was created. Both the filter and the calibration curve were recreated at the beginning of each print analyzing session. The print analysis programs were user friendly and, with practice, a print could be fully scanned, digitized, saved, and printed in approximately thirty minutes. Complete details of the Adage System Analysis can be found in Refs 1 and 2.

Color Pressure Plots and Numerical Pressure Maps

The color pressure plots were produced on the AGL VAX computer, and the numerical pressure maps were produced on the Macintosh II. The plots were produced using the procedure described by Hansen (Ref 1). The computer programs have the capability to produce two–dimensional and three-dimensional color pressure plots. These plots enhance the readability of the tire contact pressure distributions. However, the three-dimensional plots were not included in this report since they offer very little additional information.

The programs can be downloaded onto the IBM system and color plots can be generated using the IBM Professional Graphics terminal. The color pressure plots displayed by the IBM Professional Graphics monitor are clearer than those displayed by the Adage system monitor; however, it was decided not to use this feature due to the excessive amount of time required by this process.

Tire Contact Area Analysis

In order to determine the areas covered by the different pressure ranges, a computer program was written in IDL. This program, called **MAMI.PRO,** was accessed after the final **SMOOTHED.DAT** had been created by typing **@SYS$SYSTEM:IDL ADAGE @MAMI.PRO**. The areas covered by each of the pressure ranges (<50 psi, 50-100 psi, 101-150 psi, 151-200 psi, 201-250 psi, 251-300 psi, and >300 psi) were determined. Once these values were computed, the proportions of the contact area (percent of total) covered by each pressure range were calculated.

APPENDIX B. SIDE TIRE MOVEMENT DATA

Side tire deflections were recorded in order to enable any designer who uses finite-element models of tires to compare his/her results with the actual experimental values. Side tire deflections were measured for the following tires: (1) bias Goodyear 18-22.5 tire, (2) radial Michelin 275/80R/24.5 tire, (3) radial Michelin 255/70R/22.5 tire, and (4) radial Goodyear 11R24.5 tire.

Five reference points were selected on each side of the tire. These points are shown in Fig B.1. These points were chosen such that they were aligned vertically at the middle of the tire-plate contact area. The corresponding points on the other side of the tire were also selected. The data in Tables B.1 through B.8 represent the average movement of a specific reference point from its counterpart on the other side of the tire. For a vertical reference point, the vertical length of the ram-stroke was measured at a load of zero pound. The coordinates of the horizontal and vertical points, as well as the vertical length of the ram-stroke, were measured to obtain the deflection at each load.

The total tire and axle down displacement created by the load during testing and the average estimated value of the tire vertical stiffness, in lb/inch, are also included, in Tables B.1 through B.8.

THE BIAS GOODYEAR 18-22.5 SUPER SINGLE TIRE

The bias Goodyear 18-22.5 tire deflections were measured at inflation pressures of 85 and 100 psi, and at each inflation pressure the wheel was loaded to 0, 8,000, 10,000, 12,000, and 15,000 pounds. The side tire deflections for the tire inflated to 100 psi are in Table B.1, and the deflections for the tire inflated to 85 psi are in Table B.2.

THE RADIAL MICHELIN 275/80R/24.5 TIRE

The radial Michelin 275/80R/24/5 tire deflections were measured at inflation pressures of 110 and 95 psi, and at each inflation pressure the wheel was loaded to 0, 6,000, and 8,000 pounds. The side tire deflections for the tire inflated to 110 psi are in Table B.3, and the deflections for the tire inflated to 95 psi are in Table B.4.

Reference points are shown in Fig B.1. However, measurements of point 2 were not taken due to the relatively low height of this tire. The procedure described for the 18-22.5 super single tire was used for measuring the side tire movements of this tire.

THE RADIAL MICHELIN 255/70R/22.5 TIRE

The radial Michelin 255/70R/22.5 tire deflections were measured at inflation pressures of 135 and 110 psi, and at each inflation pressure the wheel was loaded to 0, 6,000, and 8,000 pounds. The side tire deflections for the tire inflated to 135 psi are in Table B.5, and the deflections for the tire inflated to 110 psi are in Table B.6.

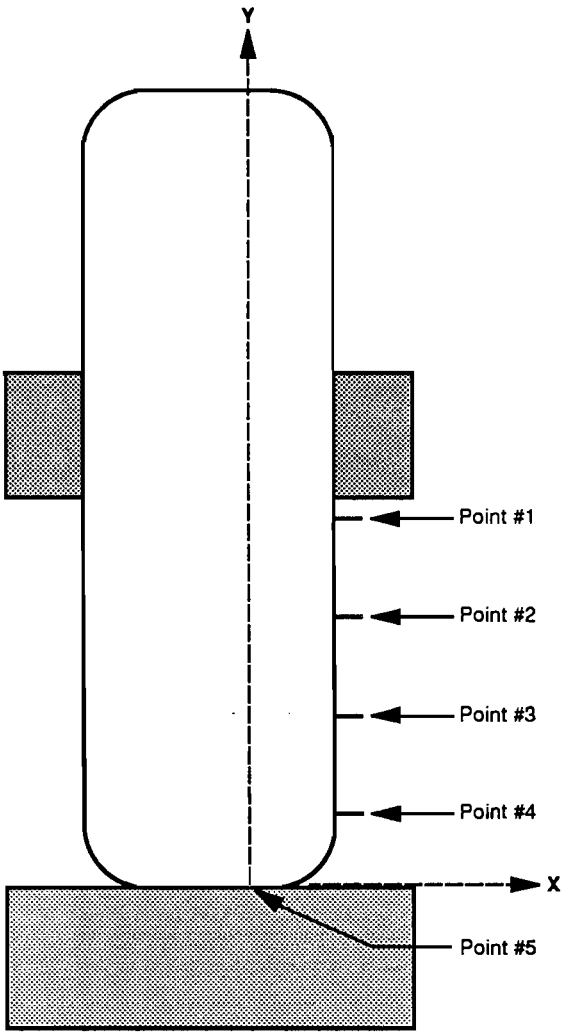

Fig B.1. Schematic of the side tire points measured for vertical and horizontal movements.

Reference points are shown in Fig B.1. However, measurements of point 2 were not taken due to the relatively low height of this tire. The procedure described for the 18-22.5 super single tire was used for measuring the side tire movements of this tire.

THE RADIAL GOODYEAR 11R24.5 TIRE

The radial Goodyear 11R24.5 tire deflections were measured at inflation pressures of 110 and 95 psi, and at each inflation pressure the wheel was loaded to 0, 6,000, and 8,000 pounds. The side tire deflections for the tire inflated to 110 psi are in Table B.7, and the deflections for the tire inflated to 95 psi are in Table B.8.

These points are shown in Fig B.1. However, measurements of point 2 were not taken due to the relatively low height of this tire. The procedure described for the 18-22.5 super single tire was used for measuring the side tire movements of this tire.

TABLE B.1. SIDE TIRE MOVEMENTS FOR THE BIAS GOODYEAR 18-22.5 SUPER SINGLE TIRE INFLATED TO 100 PSI

	Load (lb)									
	0		8,000		10,000		12,000		15,000	
Points	X*	Y*	X	Y	X	Y	X	Y	X	Y
#1	1.2	28.5	1.2	25.7	1.2	24.8	1.3	24.6	1.3	24.4
#2	4.3	22.0	4.5	18.8	4.8	18.3	4.8	18.0	5.1	17.7
#3	5.5	14.2	5.8	11.3	6.0	10.8	6.1	10.3	6.3	9.9
#4	2.2	7.5	2.6	4.8	2.9	4.6	3.0	4.2	3.2	3.8
#5	0.0	0.0	0.0	0.0	0.0	0.0	0.0	0.0	0.0	0.0
Down Axle Movement		-0.0		-3.5		-4.0		-5.1		-6.1

Average Tire Stiffness: 6,090 Pounds Per Inch

*Movements are in centimeters.

TABLE B.2. SIDE TIRE MOVEMENTS FOR THE BIAS GOODYEAR 18-22.5 SUPER SINGLE TIRE INFLATED TO 85 PSI

	Load (lb)									
	0		8,000		10,000		12,000		15,000	
Points	X*	Y*	X	Y	X	Y	X	Y	X	Y
#1	1.2	28.5	1.2	24.9	1.2	24.6	1.3	24.1	1.3	22.8
#2	4.6	22.0	4.7	18.8	4.8	18.3	5.0	17.8	5.1	16.7
#3	5.4	14.2	5.8	11.3	6.0	10.6	6.1	10.0	6.3	9.4
#4	2.4	7.5	2.9	4.7	3.0	4.5	3.1	3.9	3.2	3.5
#5	0.0	0.0	0.0	0.0	0.0	0.0	0.0	0.0	0.0	0.0
Down Axle Movement		-0.0		-3.5		-4.2		-5.3		-6.3

Average Tire Stiffness: 5,910 Pounds Per Inch

*Movements are in centimeters.

TABLE B.3. SIDE TIRE MOVEMENTS FOR THE RADIAL MICHELIN 275/80R/24.5 TIRE INFLATED TO 110 PSI

	Load (lb)					
	0		6,000		8,000	
Points	X*	Y*	X	Y	X	Y
#1	2.7	20.2	2.7	18.4	2.7	17.8
#3	3.5	11.3	5.1	8.8	5.4	8.1
#4	2.7	5.2	2.9	4.6	3.7	4.4
#5	0.0	0.0	0.0	0.0	0.0	0.0
Down Axle Movement		-0.0		-3.0		-4.1

Average Tire Stiffness: 5,020 Pounds Per Inch

*Movements are in centimeters.

TABLE B.4. SIDE TIRE MOVEMENTS FOR THE RADIAL MICHELIN 275/80R/24.5 TIRE INFLATED TO 95 PSI

	Load (lb)					
	0		6,000		8,000	
Points	X*	Y*	X	Y	X	Y
#1	2.7	20.1	2.7	18.0	2.7	17.0
#3	3.8	11.3	5.3	8.5	5.8	7.9
#4	2.7	5.2	2.9	4.3	3.8	4.0
#5	0.0	0.0	0.0	0.0	0.0	0.0
Down Axle Movement		-0.0		-3.0		-4.1

Average Tire Stiffness: 4,420 Pounds Per Inch

*Movements are in centimeters.

TABLE B.5. SID ETIRE MOVEMENTS FOR THE RADIAL MICHELIN 255/70R/22.5 TIRE INFLATED TO 135 PSI

	Load (lb)					
	0		6,000		8,000	
Points	X*	Y*	X	Y	X	Y
#1	1.1	16.9	1.1	14.3	1.1	13.5
#3	2.8	6.8	3.5	96.4	3.9	6.0
#4	1.6	4.5	2.0	4.2	2.3	3.3
#5	0.0	0.0	0.0	0.0	0.0	0.0
Down Axle Movement		-0.0		-3.1		-3.8

Average Tire Stiffness: 5,140 Pounds Per Inch

*Movements are in centimeters.

TABLE B.6. SIDE TIRE MOVEMENTS FOR THE RADIAL MICHELIN 255/70R/22.5 TIRE INFLATED TO 110 PSI

	Load (lb)					
	0		6,000		8,000	
Points	X*	Y*	X	Y	X	Y
#1	1.1	17.0	1.1	13.7	1.1	12.9
#3	2.7	7.0	3.9	6.2	4.4	5.4
#4	1.6	4.5	2.2	3.0	2.5	2.7
#5	0.0	0.0	0.0	0.0	0.0	0.0
Down Axle Movement		-0.0		-3.4		-4.3

Average Tire Stiffness: 4,610 Pounds Per Inch

*Movements are in centimeters.

TABLE B.7. SIDE TIRE MOVEMENTS FOR THE RADIAL GOODYEAR 11R24.5 TIRE INFLATED TO 110 PSI

	Load (lb)					
	0		6,000		8,000	
Points	X*	Y*	X	Y	X	Y
#1	3.1	22.5	3.1	20.0	3.1	19.1
#3	4.2	12.9	5.6	9.2	5.8	8.8
#4	3.9	7.0	4.5	6.4	4.8	5.9
#5	0.0	0.0	0.0	0.0	0.0	0.0
Down Axle Movement		-0.0		-3.0		-4.1

Average Tire Stiffness: 5,020 Pounds Per Inch

*Movements are in centimeters.

TABLE B.8. SIDE TIRE MOVEMENTS FOR THE RADIAL GOODYEAR 11R24.5 TIRE INFLATED TO 95 PSI

	Load (lb)					
	0		6,000		8,000	
Points	X*	Y*	X	Y	X	Y
#1	3.1	22.4	3.1	19.5	3.1	18.8
#3	4.2	12.8	5.7	9.0	5.9	8.5
#4	3.9	6.9	4.7	6.2	4.9	5.8
#5	0.0	0.0	0.0	0.0	0.0	0.0
Down Axle Movement		-0.0		-3.4		-4.3

Average Tire Stiffness: 4,600 Pounds Per Inch

*Movements are in centimeters.